Quantum Coding Bounds and a Closed-Form Approximation of the Minimum Distance versus Quantum Coding Rate

Daryus Chandra, *Student Member, IEEE,* Zunaira Babar, Hung Nguyen, *Member, IEEE,* Dimitrios Alanis, *Student Member, IEEE,* Panagiotis Botsinis, *Member, IEEE,* Soon Xin Ng, *Senior Member, IEEE,* and Lajos Hanzo *Fellow, IEEE,*

***Abstract*—The trade-off between the quantum coding rate and the associated error correction capability is characterized by the quantum coding bounds. The unique solution for this trade-off does not exist, but the corresponding lower and the upper bounds can be found in the literature. In this treatise, we survey the existing quantum coding bounds and provide new insights into the classical to quantum duality for the sake of deriving new quantum coding bounds. Moreover, we propose an appealingly simple and invertible analytical approximation, which describes the trade-off between the quantum coding rate and the minimum distance of quantum stabilizer codes. For example, for a half-rate quantum stabilizer code having a codeword length of $n = 128$, the minimum distance is bounded by $11 < d < 22$, while our formulation yields a minimum distance of $d = 16$ for the above-mentioned code. Ultimately, our contributions can be used for the characterization of quantum stabilizer codes.**

***Index Terms*—Quantum error correction codes, quantum stabilizer codes, quantum coding bound**

I. Introduction

Moore's Law has remained valid for five decades, but based on its prediction at the time of writing the classical integrated circuits are expected to enter the nano-scale domain, where the laws of quantum mechanics prevail [1], [2]. Quantum computers potentially offer substantial benefits over classical computers owing to their inherent parallel processing capability [3]–[14]. However, quantum computers are susceptible to the deleterious effect of quantum decoherence. Hence, quantum error correction codes (QECCs) have been proposed for correcting the bit-flips and phase-flips imposed by the decoherence effects. Furthermore, the employment of QECC in quantum computers is also capable of extending the coherence time of qubits [15]. The concept of protecting quantum information is similar to that of its classical counterpart by attaching redundancy to the information, which is then invoked later for error correction. The quest for finding the "good" QECCs was inspired by Shor, who introduced the 9-qubit code, which is often referred to as the Shor's code [16]. Shor's code encodes a single information qubit, which is also referred to as "logical qubit", into nine encoded qubits or "physical qubits". The Shor's code construction is capable of protecting the nine physical qubits from any type of single qubit error. Following the discovery of Shor's code, another QECC scheme, namely the Steane's code, was proposed [17]. The latter is capable of protecting any single qubit error by encoding a single logical qubit into seven physical qubits, instead of nine qubits. The question about what the minimum number of physical qubits is required in order to protect the physical qubits from any type of single qubit error was answered when Laflamme *et al.* proposed the 5-qubit quantum code [18]. This 5-qubit code may be referred to as Laflamme's code or also shown as the "perfect code", since the code construction achieves the quantum Hamming bound, which is the upper bound of quantum coding rate given the minimum diatance of any QECC construction [19], [20].

The field of QECCs entered its golden age following the invention of quantum stabilizer codes (QSCs) [21], [22]. The QSC paradigm allows us to transform the classical error correction codes into their quantum counterparts. The QSCs also circumvent the problem of estimating both the number and the position of quantum-domain errors imposed by quantum decoherence without observing the actual quantum states, since observing the quantum states would collapse the qubits into classical bits. This extremely beneficial error estimation was achieved by introducing the syndrome-measurement based approach [21], [22]. In classical error correction codes, the syndrome-measurement based approach has been widely exploited for invoking the error detection and correction procedure. Therefore, the formulation of QSCs expanded the search space of good QECCs to a broader horizon. This new paradigm of incorporating the classical to quantum isomorphisms, led to the transformation of classical codes to their quantum domain duals, such as Quantum Bose-Chaudhuri-Hocquenghem (QBCH) codes [23], [24], Quantum Reed-Solomon (QRS) codes [25], Quantum Reed-Muller (QRM) codes [26], Quantum Convolutional Codes (QCC) [27], [28], Quantum Low-Density Parity-Check (QLDPC) codes [29], Quantum Turbo Codes (QTC) [30] and Quantum Polar Codes (QPC) [31]. Apart from exploiting the above isomorphism, there are also significant contributions on directly developing code constructions solely based on the pure quantum topology and homology, as exemplified by the family of toric

The authors are with the School of Electronics and Computer Science, University of Southampton, Southampton, SO17 1BJ, UK (email: {dc2n14, zb2g10, hvn08r, da4g11, pb1y14, sxn, lh}@ecs.soton.ac.uk).

The financial support of the EPSRC under the grant EP/L018659/1, that of the European Research Council, Advanced Fellow Grant and that of the Royal Society's Wolfson Research Merit Award is gratefully acknowledged. Additionally, the authors acknowledge the use of the IRIDIS High Performance Computing Facility, and associated support services at the University of Southampton, in the completion of this work.

	List of Acronyms
CNOT	Controlled-NOT
CSS	Calderbank-Shor-Steane
EA	Entanglement-Assisted
GV	Gilbert-Varshamov
PCM	Parity Check Matrix
QBCH	Quantum Bose-Chaudhuri-Hocquenghem
QBER	QuBit Error Rate
QECC	Quantum Error Correction Code
QGF(4)	Quantum code from $GF(4)$
QRM	Quantum Reed-Muller
QSC	Quantum Stabilizer Code

	List of Symbols
c	Number of Preshared Entangled Pair of Qubits
d	Minimum Distance
d_{ea}	Minimum Distance of Entanglement-Assisted Code
E	Entanglement Consumption Rate
$\mathcal{E}$	Pauli Error Pattern
$\mathbf{e}$	Error Vector
g	Stabilizer Operator
$\mathbf{G}$	Generator Matrix
$H(x)$	Binary Entropy of x
$\mathbf{H}$	Parity Check Matrix, Hadamard Transformation
k	Information Bit Length, Number of Logical Qubits
n	Codeword Length, Number of Physical Qubits
r	Classical Coding Rate
r_Q	Quantum Coding Rate
$\mathbf{s}$	Syncrome Vector
t	Error Correction Capability
U	Unitary Transformation
δ	Normalized Minimum Distance
θ	Entanglement Ratio
$\otimes$	Kronecker Tensor Product
$\vert\psi\rangle$	Quantum State ψ

codes [32]–[34], surface codes [35], [36], colour codes [37], cubic codes [38], hyperbolic surface codes [39], [40], hyperbolic color codes [41], hypergraph product codes [42]–[44] and homological product codes [45]. A timeline that portrays the milestones of QSCs, at a glance is depicted in Fig. 1. Although the QSC formulation creates an important class of QECCs, we note that there are also other classes of QECCs beside the QSCs, such as the class of decoherence-free subspace (DFS) codes. DFS codes can be viewed as passive QECCs, while the QSCs are a specific example of the active ones. To elaborate a little further, DFS codes constitute a highly degenerate class of QECCs, which rely on the fact that the error patterns may preserve the state of physical qubits and therefore they do not neccessarily require a recovery procedure [46]. Due to their strong reliance on the degeneracy property exhibited by QECCs without a classical counterpart, the class of DFS codes bears no resemblance to any classical error correction codes. Therefore, in this treatise we focus our discussions purely on QSCs, which exhibit strong analogies with classical error correction codes.

Even though intensive research efforts have been invested in exploring the QSCs field, one of the mysteries still remains unresolved. Since the development of the first QSC, one of the open problems has been how to determine the realistically achievable size of the codebook $|\mathcal{C}| = 2^k$, given the number of physical qubits n, the minimum distance of d, and the quantum coding rate of $r_Q = k/n$, where k denotes the number of logical qubits. The minimum distance d is the parameter that defines the error correction capability of the corresponding code. The complete formulation of the realistically achievable minimum distance d, given the number of physical qubits n and the quantum coding rate r_Q is unknown at the time of writing, but several theoretical lower and upper bounds can be found in the literature. Naturally, finding code constructions associated with growing minimum distances upon reducing the coding rate is desirable, since an increased minimum distance improves the reliability of quantum computation [60]–[64]. From the implementational perspective, the so-called quantum topological codes are popular in the field of fault-tolerant quantum computing. Nonetheless, one of the substantial drawbacks of quantum topological codes is their potentially very low quantum coding rate, tends towards zero

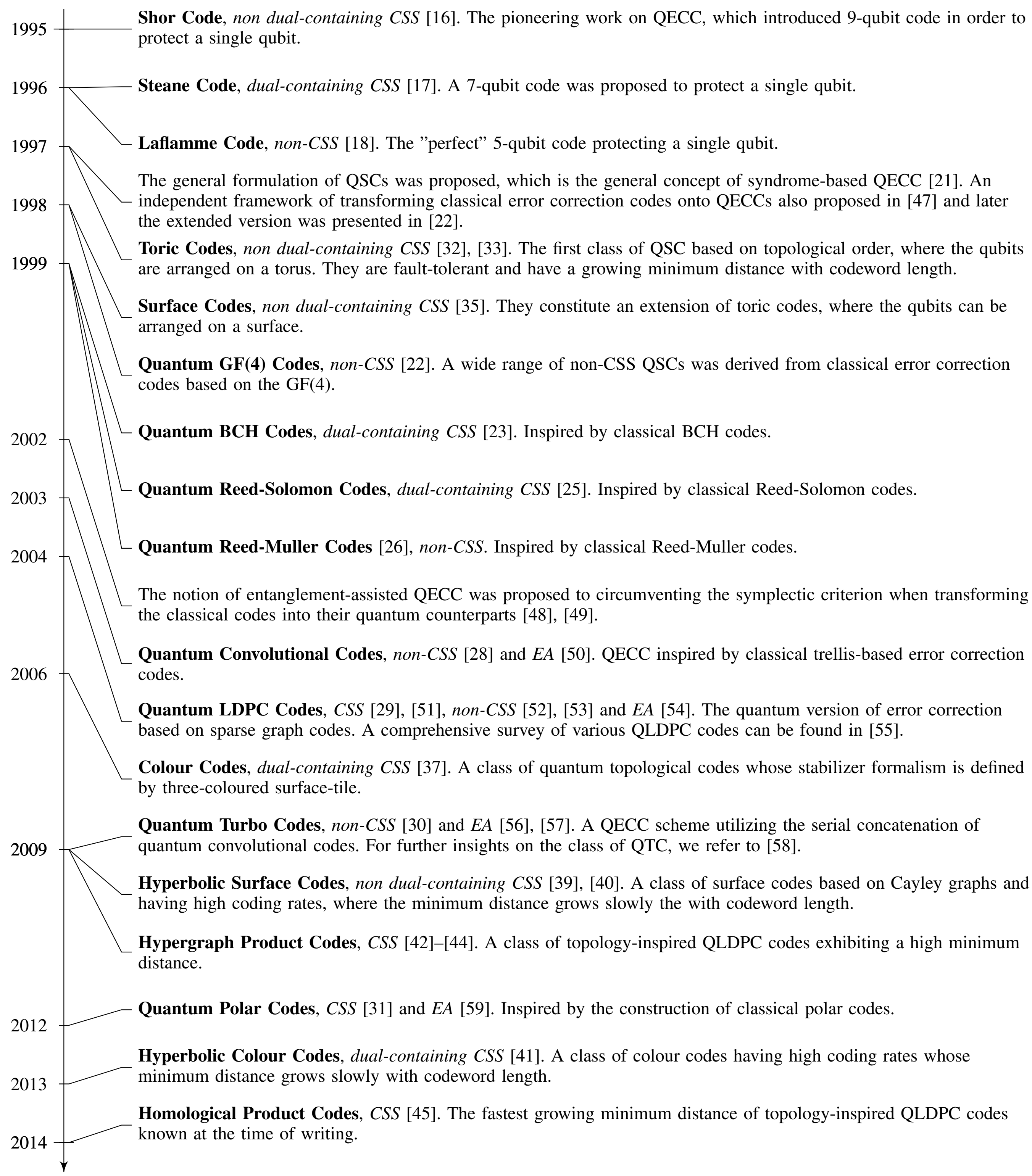

Fig. 1: Timeline of important milestones in QECC field, specifically in the development of QSCs. The code construction is highlighted with **bold** fonts, while the associated code type is printed in *italics*.

for long codewords. Another class suitable for fault-tolerant QSCs is constituted by the family of QLDPC codes, which is a benefit of their sparse parity check matrices (PCMs), since the sparseness of the PCM guarantees having a limited error propagation of the qubits within a codeword. Although the QLDPC codes are capable of achieving a good performance at an adequate coding rate, they actually have a modest minimum distance [29]. The trade-off between the quantum coding rate and the minimum distance as well as the codeword length is widely recognized, but the achievable minimum distance d of a quantum code given the quantum coding rate r_Q and codeword length n still remained unresolved. For example, for a given codeword length of $n = 128$ and quantum coding rate of $r_Q = 1/2$, the achievable minimum distance is losely bounded by $11 < d < 22$, while for $n = 1024$ and $r_Q = 1/2$, the achievable minimum distance is bounded by $78 < d < 157$. Naturally, having such a wide range of minimum distance is undesirable. For binary classical codes, this problem has been circumvented by the closed-form approximation proposed by Akhtman *et al* [65].

The challenge of creating the quantum counterpart of error correction codes lies in the fact that QSC constructions have to mitigate not only bit-flip errors, but also phase-flip errors or in fact both bit-flip and phase-flip errors. Based on how we mitigate those different types of errors, we can simply categorize QSCs as being in the class of Calderbank-Shor-Steane (CSS) codes [17], [66], [67] or as being non-CSS codes [22]. The CSS codes handle the qubit errors by treating the bit-flip errors and phase-flip errors as separate entities. By contrast, the class of non-CSS codes treat both bit-flip errors and phase-flip errors simultaneously. Since the CSS codes treat the bit-flip and phase-flip error correction procedures separately, in general, they exhibit a lower coding rate than their non-CSS counterparts having the same error correction capability. Furthermore, if we also consider the presence of quantum entanglement, we may conceive more powerful quantum code constructions. To elaborate, the family of entanglement-assisted quantum stabilizer codes (EA-QSCs) is capable of operating at a higher quantum coding rate than the unassisted QSC constructions at a given error correction capability, provided that error-free maximally-entangled qubits have already been preshared [48], [49].

Against this background, our contributions are summarized as follows:

- *We provide a survey of the existing quantum coding bounds found in the literature, along with their relationship to the existing quantum stabilizer code constructions. Moreover, to bridge the gap between the classical and quantum coding bounds, we provide further insights into the classical to quantum isomorphism in the context of the associated coding bound formulations.*
- *We formulate a simple invertible formulation of $r(n, \delta)$ characterizing the relationship between the quantum coding rate and the associated achievable minimum distance of quantum stabilizer codes. The resultant closed-form approximation of quantum coding bound is suitable both for idealized infinite and practical finite-length codewords. More specifically, we show that using our closed-form approximation, we become able to estimate the realistically achievable minimum distance of quantum stabilizer codes.*
- *We then derive the bounds for maximally-entangled quantum stabilizer codes in conjunction with arbitrary entanglement ratios and relate them to those of unassisted quantum stabilizer codes. More explicitly, for the entanglement ratio of $\theta = 0$, we arrive at the bounds of unassisted quantum stabilizer codes while for $\theta = 1$, we generate the quantum coding bounds for their maximally-entangled counterparts.*

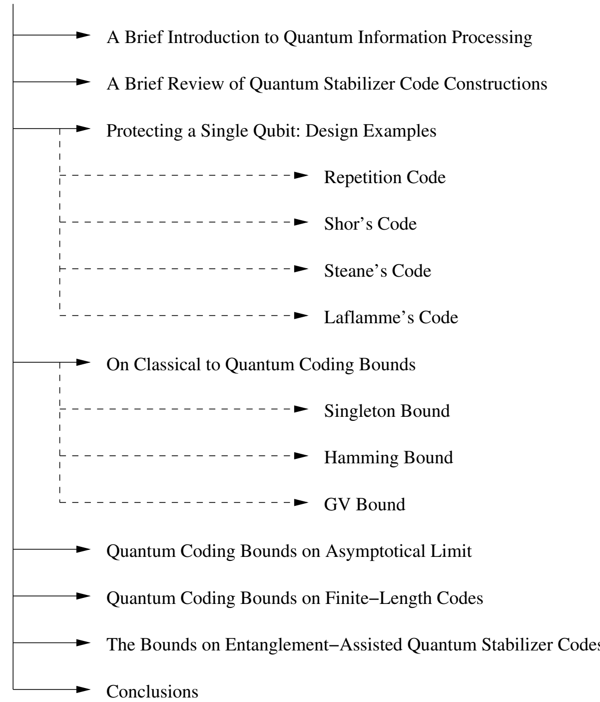

Fig. 2: The structure of the paper.

The structure of the paper is described in Fig. 2 and the rest of this paper is organized as follows. In Section II, we commence with a brief fundamentals background on quantum states. A review of QSC constructions is presented in Section III, followed by Section IV, where we illustrate the Pauli-to-Binary isomorphism in the context of QSCs that are capable of correcting single qubit errors. By incorporating the classical to quantum duality, we show how to derive quantum coding bounds from their classical counterparts and we also contrast them in Section V. We then proceed with the study of quantum coding bounds derived both for asymptotical infinite and practical finite-length codewords in Section VI and Section VII, respectively. We then provide further insights into the quantum coding bounds of entanglement-assisted quantum stabilizer codes in Section VIII. Finally, we conclude in Section IX.

II. A Brief Introduction to Quantum Information Processing

In classical computation, the information is conveyed by a binary digit or "bit". Each bit has a value of either logical "0" or "1". Similarly, in a quantum computer, a single element of information is represented by a quantum bit (qubit). Each of the qubits is in a superposition of the "0" and "1". The state of a single qubit can be represented mathematically as

$$|\psi\rangle = \alpha_0|0\rangle + \alpha_1|1\rangle, \tag{1}$$

where we have $\alpha_0, \alpha_1 \in \mathbb{C}$ and $|\alpha_0|^2 + |\alpha_1|^2 = 1$. For a single qubit in the state of Eq. (1), the probability of obtaining $|0\rangle$ upon observation is $P_0 = |\alpha_0|^2$ and for the state $|1\rangle$, it is $P_1 = |\alpha_1|^2$. Representing the state of a qubit as shown in Eq. (1) is also known as the Dirac notation or "bra-ket" notation [68]. Apart from using the Dirac notation, we may represent the state of a single qubit as a 2-component vector as follows:

$$\begin{aligned}|\psi\rangle &= \alpha_0|0\rangle + \alpha_1|1\rangle \\ &= \alpha_0\begin{pmatrix}1\\0\end{pmatrix} + \alpha_1\begin{pmatrix}0\\1\end{pmatrix} \\ &= \begin{pmatrix}\alpha_0\\ \alpha_1\end{pmatrix}. \end{aligned} \tag{2}$$

Basically, a single qubit system may be viewed as a two-component vector in the two-dimensional Hilbert space and correspondingly an N-qubit string lies within the 2^N-dimensional Hilbert space. More specifically, for example, a two-qubit operand is in a superposition of four states of 00, 01, 10, and 11 simultaneously, which can be written as

$$|\psi\rangle = \alpha_{00}|00\rangle + \alpha_{01}|01\rangle + \alpha_{10}|10\rangle + \alpha_{11}|11\rangle, \tag{3}$$

where the constraints of $\alpha_{00}, \alpha_{01}, \alpha_{10}, \alpha_{11} \in \mathbb{C}$ and $|\alpha_{00}|^2 + |\alpha_{01}|^2 + |\alpha_{10}|^2 + |\alpha_{11}|^2 = 1$ still hold. If the binary representations of 00, 01, 10 and 11 are translated to their decimal representations of 0, 1, 2 and 3 respectively, the resultant N-qubit state can be encapsulated as

$$|\psi\rangle = \sum_{i=0}^{2^N-1} \alpha_i|i\rangle \text{ where } \alpha_i \in \mathbb{C}, \sum_{i=0}^{2^N-1} |\alpha_i|^2 = 1. \tag{4}$$

The Pauli group $\mathcal{G}_1$ defines the unitary transformation of a single qubit, which is closed under multiplication. The Pauli group $\mathcal{G}_1$ is defined as

$$\mathcal{G}_1 = \{eP : P \in \{\mathbf{I}, \mathbf{X}, \mathbf{Y}, \mathbf{Z}\}, e \in \{\pm 1, \pm i\}\}, \tag{5}$$

where $\mathbf{I}$, $\mathbf{X}$, $\mathbf{Y}$ and $\mathbf{Z}$ are the Pauli matrices, which manipulate the two-dimensional single qubit state and each of them is defined as follows:

$$\begin{aligned}\mathbf{I} &= \begin{pmatrix}1 & 0\\0 & 1\end{pmatrix}, \quad \mathbf{X} = \begin{pmatrix}0 & 1\\1 & 0\end{pmatrix}, \\ \mathbf{Y} &= \begin{pmatrix}0 & -i\\i & 0\end{pmatrix}, \quad \mathbf{Z} = \begin{pmatrix}1 & 0\\0 & -1\end{pmatrix}.\end{aligned} \tag{6}$$

In the context of quantum information processing, each Pauli matrix represents the discrete set of errors that may corrupt a single qubit state. Physically, they represent a bit-flip error ($\mathbf{X}$), a phase-flip error ($\mathbf{Z}$), as well as a joint bit-flip and phase-flip error ($i\mathbf{XZ} = \mathbf{Y}$), while Pauli-$\mathbf{I}$ represents the identity operator corresponding to the absence of errors. However, it is always important to bear in mind that the nature of quantum decoherence is continuous and it can be modeled as a linear combination of $\mathbf{X}$, $\mathbf{Z}$, and $\mathbf{Y}$ type errors. Fortunately, due to the effect of stabilizer measurement, we can model the continuous nature of quantum decoherence with the aid of the bit-flip ($\mathbf{X}$), phase-flip ($\mathbf{Z}$), as well as a simultaneous bit-flip and phase flip ($\mathbf{Y}$) errors.

For an N-qubit operator, the general Pauli group $\mathcal{G}_n$ is represented by an n-fold tensor product of $\mathcal{G}_1$, as defined below:

$$\mathcal{G}_n = \{P_1 \otimes P_2 \cdots \otimes P_n | P_j \in \mathcal{G}_1\}. \tag{7}$$

The Pauli channel inflicts an error $\mathcal{P} \in \mathcal{G}_n$ on an N-qubit string, where each qubit may independently experience either a bit-flip error ($\mathbf{X}$), a phase-flip error ($\mathbf{Z}$), or both bit-flip and phase-flip error ($i\mathbf{XZ} = \mathbf{Y}$). For instance, let us assume having a single qubit in the state of $|\psi\rangle = \alpha_0|0\rangle + \alpha_1|1\rangle$. A Pauli matrix $\mathbf{X}$ transforms a single qubit in the state of $|\psi\rangle$ into the following state:

$$\begin{aligned}|\psi'\rangle &= \mathbf{X}|\psi\rangle \\ &= \begin{pmatrix}0 & 1\\1 & 0\end{pmatrix} \cdot \begin{pmatrix}\alpha_0\\ \alpha_1\end{pmatrix} \\ &= \begin{pmatrix}\alpha_1\\ \alpha_0\end{pmatrix} \\ &\equiv \alpha_1|0\rangle + \alpha_0|1\rangle.\end{aligned} \tag{8}$$

The transformation by the Pauli matrix $\mathbf{Z}$ of a single qubit state results in a phase-flip, which is defined by

$$\begin{aligned}|\psi'\rangle &= \mathbf{Z}|\psi\rangle \\ &= \begin{pmatrix}1 & 0\\0 & -1\end{pmatrix} \cdot \begin{pmatrix}\alpha_0\\ \alpha_1\end{pmatrix} \\ &= \begin{pmatrix}\alpha_0\\ -\alpha_1\end{pmatrix} \\ &\equiv \alpha_0|0\rangle - \alpha_1|1\rangle.\end{aligned} \tag{9}$$

By following the same method, we can readily determine the manipulated state of a single qubit by the Pauli matrix $\mathbf{Y}$ resulting both in a simultaneous bit-flip and phase-flip as follows:

$$\begin{aligned}|\psi'\rangle &= \mathbf{Y}|\psi\rangle \\ &= \begin{pmatrix}0 & -i\\i & 0\end{pmatrix} \cdot \begin{pmatrix}\alpha_0\\ \alpha_1\end{pmatrix} \\ &= \begin{pmatrix}i\alpha_1\\ -i\alpha_0\end{pmatrix} \\ &\equiv i\alpha_1|0\rangle - i\alpha_0|1\rangle,\end{aligned} \tag{10}$$

Let us now proceed by applying the unitary transformation to a multi-qubit state of Eq. 7. For instance, let us assume a two-qubit operand in the state of Eq. 3, which can be represented as a 4-element vector as follows:

$$|\psi\rangle = \begin{pmatrix}\alpha_{00}\\ \alpha_{01}\\ \alpha_{10}\\ \alpha_{11}\end{pmatrix}. \tag{11}$$

For example, the quantum decoherence inflicts the two-qubit unitary transformation of $(\mathbf{X} \otimes \mathbf{I})$[1] upon a two-qubit state,

[1]For the sake of simplifying the notation, a set of Pauli matrices for defining a multi-qubit unitary transformation usually does not include the "$\otimes$" operator. For example, a unitary transformation ($\mathbf{X} \otimes \mathbf{Z} \otimes \mathbf{X} \otimes \mathbf{I}$) acting upon a 4-qubit operand can simply be rewritten as $\mathbf{XZXI}$. In the rest of the paper, the latter representation is used.

which can be described as follows:

$$
\begin{aligned}
|\psi'\rangle &= (\mathbf{X}\otimes\mathbf{I})\,|\psi\rangle \\
&= \left(\begin{pmatrix} 0 & 1 \\ 1 & 0 \end{pmatrix} \otimes \begin{pmatrix} 1 & 0 \\ 0 & 1 \end{pmatrix}\right) \cdot \begin{pmatrix} \alpha_{00} \\ \alpha_{01} \\ \alpha_{10} \\ \alpha_{11} \end{pmatrix} \\
&= \begin{pmatrix} 0 & \begin{pmatrix} 1 & 0 \\ 0 & 1 \end{pmatrix} \\ \begin{pmatrix} 1 & 0 \\ 0 & 1 \end{pmatrix} & 0 \end{pmatrix} \cdot \begin{pmatrix} \alpha_{00} \\ \alpha_{01} \\ \alpha_{10} \\ \alpha_{11} \end{pmatrix} \\
&= \begin{pmatrix} 0 & 0 & 1 & 0 \\ 0 & 0 & 0 & 1 \\ 1 & 0 & 0 & 0 \\ 0 & 1 & 0 & 0 \end{pmatrix} \cdot \begin{pmatrix} \alpha_{00} \\ \alpha_{01} \\ \alpha_{10} \\ \alpha_{11} \end{pmatrix} \\
&= \begin{pmatrix} \alpha_{10} \\ \alpha_{11} \\ \alpha_{00} \\ \alpha_{01} \end{pmatrix} \\
&\equiv \alpha_{10}|00\rangle + \alpha_{11}|01\rangle + \alpha_{00}|10\rangle + \alpha_{01}|11\rangle.
\end{aligned} \tag{12}
$$

The final state of Eq. (12) can also be obtained without expanding the tensor product of the unitary transformation by flipping the state of the first qubit, since the unitary transformation of $\mathbf{XI}$ means that a bit-flip error occurs on the first qubit, while the second qubit does not experience any impairment. More explicitly, due to the unitary transformation $\mathbf{XI}$, the state of $|00\rangle$ is changed to state of $|10\rangle$. The same transformation is also applied to the states of $|01\rangle$, $|10\rangle$, and $|11\rangle$, where they are transformed to the states of $|11\rangle$, $|00\rangle$, $|10\rangle$, respectively. Hence, the magnitude associated with the state of $|00\rangle$ is no longer α_{00} and now it becomes α_{10}. Therefore, the magnitudes associated with the states of $|01\rangle$, $|10\rangle$, and $|11\rangle$ are α_{11}, α_{00}, and α_{01}, respectively.

Since we focus our discussions on the family of QSCs, the quantum coding bounds can be derived from their classical counterparts. Even though most of the well-known bounds on quantum codes are derived on the basis of the classical-to-quantum isomorphism, the pure quantum code constructions not relying on the classical-to-quantum isomorphism, but rather based on topological and homological orders still obey to these quantum coding bounds, provided that they belong to the family of non-degenerate quantum codes. To elaborate a little further, degeneracy is one of the distinctive characteristics of quantum codes, which cannot be found in their classical counterpart. More explicitly, quantum codes inherently exhibit a degeneracy property implying that different error patterns of $\mathcal{P} \in \mathcal{G}_n$ may yield an identical corrupted state. For example, let us assume a two-qubit operand in the following state:

$$|\psi\rangle = \frac{1}{\sqrt{2}}\left(|00\rangle + |11\rangle\right), \tag{13}$$

and consider two different error patterns, which can be described as a pair of two-qubit unitary transformations given by $\mathcal{E}_1 = \mathbf{IZ}$ and $\mathcal{E}_2 = \mathbf{ZI}$. The resultant state after the error pattern $\mathcal{E}_1$ is imposed to the two-qubit system can be described as follows:

$$
\begin{aligned}
|\psi'_1\rangle &= \mathbf{IZ}|\psi\rangle \\
&= \begin{pmatrix} 1 & 0 & 0 & 0 \\ 0 & -1 & 0 & 0 \\ 0 & 0 & 1 & 0 \\ 0 & 0 & 0 & -1 \end{pmatrix} \cdot \begin{pmatrix} \frac{1}{\sqrt{2}} \\ 0 \\ 0 \\ \frac{1}{\sqrt{2}} \end{pmatrix} = \begin{pmatrix} \frac{1}{\sqrt{2}} \\ 0 \\ 0 \\ -\frac{1}{\sqrt{2}} \end{pmatrix} \\
&\equiv \frac{1}{\sqrt{2}}\left(|00\rangle - |11\rangle\right),
\end{aligned} \tag{14}
$$

while the acts of $\mathcal{E}_2$ upon the state of $|\psi\rangle$ will result in the following state:

$$
\begin{aligned}
|\psi'_2\rangle &= \mathbf{ZI}|\psi\rangle \\
&= \begin{pmatrix} 1 & 0 & 0 & 0 \\ 0 & 1 & 0 & 0 \\ 0 & 0 & -1 & 0 \\ 0 & 0 & 0 & -1 \end{pmatrix} \cdot \begin{pmatrix} \frac{1}{\sqrt{2}} \\ 0 \\ 0 \\ \frac{1}{\sqrt{2}} \end{pmatrix} = \begin{pmatrix} \frac{1}{\sqrt{2}} \\ 0 \\ 0 \\ -\frac{1}{\sqrt{2}} \end{pmatrix} \\
&\equiv \frac{1}{\sqrt{2}}\left(|00\rangle - |11\rangle\right).
\end{aligned} \tag{15}
$$

Since the error patterns $\mathcal{E}_1 = \mathbf{IZ}$ and $\mathcal{E}_2 = \mathbf{ZI}$ yield an identical corrupted states $|\psi'_1\rangle$ and $|\psi'_2\rangle$, they undoubtly require an identical recovery procedure. Indeed, exploiting the degeneracy property may potentially increase the error correction capability of quantum codes. However, the question as to whether there exist degenerate quantum codes that are capable of operating beyond the quantum Hamming bound remains unresolved at the time of writing. Therefore, we limit our discussions in this treatise to the non-degenerate QSCs, although some research on finding the bounds of degenerate quantum codes can be found in [19], [69], [70].

III. A Brief Review of Quantum Stabilizer Code Constructions

Let us recall the fact that qubits collapse to classical bits upon measurement [71]. This prevents us from directly transplanting the classical error correction procedures to the quantum domain. Inspired by the PCM-based syndrome decoding philosophy, the notion of QSCs was introduced in [21], where the terminology of *quantum stabilizer codes* (QSCs) represents the quantum domain counterpart of syndrome-based classical error correction codes. Almost at the same time, an independent framework of transforming classical error correction codes to QECCs was proposed in [47] and later the extended version was presented in [22]. The aforementioned proposals are similar in terms of their concept and the terminology of *quantum stabilizer codes* (QSCs) is widely recognized, unifying both framewoks. The QSCs formulation allows us to transform every PCM-based classical error correction code into its quantum counterpart. Considering that QSCs have to handle several different types of errors, namely bit-flip errors ($\mathbf{X}$), phase-flip errors ($\mathbf{Z}$), as well as both bit-flip and phase-flip errors ($i\mathbf{XZ} = \mathbf{Y}$), the PCM of $\mathcal{C}[n,k]$[2] of QSCs, in

[2]To avoid ambiguity concerning the classical and quantum coding notation, the notation $\mathcal{C}(n,k)$ will be used to address classical codes and $\mathcal{C}[n,k]$ for quantum codes.

general, can be formulated as

$$\mathbf{H} = (\mathbf{H}_z|\mathbf{H}_x). \tag{16}$$

The stabilizer formalism given in Eq. (16), can be interpreted as a pair of binary PCMs $\mathbf{H}_z$ and $\mathbf{H}_x$. However, a pair of $\mathbf{H}_z$ and $\mathbf{H}_x$ only can be translated into quantum stabilizer codes, if they satisfy the *symplectic criterion* given by [21], [22]

$$\mathbf{H}_z\mathbf{H}_x^T + \mathbf{H}_x\mathbf{H}_z^T = 0. \tag{17}$$

The CSS codes constitute a special class of QSCs. More specifically, the construction of a $\mathcal{C}[n, k_1 - k_2]$ CSS code, which is capable of correcting t qubit errors including the bit-flip as well as phase-flip errors, can be derived from the pair of classical linear block codes $\mathcal{C}_1(n_1, k_1)$ and $\mathcal{C}_2(n_2, k_2)$ if $\mathcal{C}_2 \subset \mathcal{C}_1$, where both $\mathcal{C}_1$ and the dual pair of $\mathcal{C}_2$[3], denoted by $\mathcal{C}_2^\perp$, are capable of correcting t bit errors. For the CSS code constructions, the PCM $\mathbf{H}_z$ is obtained from the PCM of $\mathcal{C}_1$ invoked for handling bit-flip errors, while the the PCM $\mathbf{H}_x$ is obtained from the dual $\mathcal{C}_2^\perp$ is used for correcting the phase-flip errors. Since the phase-flip and bit-flip errors are treated separately in quantum CSS code constructions, the corresponding PCMs for stabilizer matrices of $\mathbf{H}_z$ and $\mathbf{H}_x$ are given by $\mathbf{H}_z = \begin{pmatrix} \mathbf{H}_z' \\ 0 \end{pmatrix}$ and $\mathbf{H}_x = \begin{pmatrix} 0 \\ \mathbf{H}_x' \end{pmatrix}$, respectively. Consequently, the binary PCM $\mathbf{H}$ is defined as

$$\mathbf{H} = \left(\begin{array}{c|c} \mathbf{H}_z' & \mathbf{0} \\ \mathbf{0} & \mathbf{H}_x' \end{array} \right). \tag{18}$$

Moreover, since we have $\mathcal{C}_2 \subset \mathcal{C}_1$, the symplectic criterion of Eq. (17) can be reduced to $\mathbf{H}_z'\mathbf{H}_x'^T = 0$. Furthermore, if the construction satisfies $\mathbf{H}_z' = \mathbf{H}_x'$, the resultant codes are defined as dual-containing quantum CSS codes, or self-orthogonal quantum CSS codes because $\mathbf{H}_z'\mathbf{H}_z'^T = 0$, or equivalent to $\mathcal{C}_1^\perp \subset \mathcal{C}_1$.

Again, the classical code constructions can be readily transformed into their quantum version provided that they satisfy the symplectic criterion of Eq. (17). The latter constraint prevents us from transplanting some well-known classical codes into the quantum domain. However, fortunately this limitation can be relaxed by utilizing the family of entanglement-assisted quantum stabilizer codes (EA-QSCs) [48], [49]. The luxury of being able to transform every type of classsical codes into quantum codes does not come without cost. Invoking the EA-QSC construction requires preshared maximally-entangled qubits before encoding procedure as detailed in [49]. However, the mechanism of presharing the maximally-entangled qubits allows us to transform a set of non-symplectic QSCs into their symplectic counterpart. For a crystal clear illustration, the classification and characterization of the QSCs is summarized in Fig. 3. For more a detailed history and important milestones of the QSCs field, please refer to [55], [58].

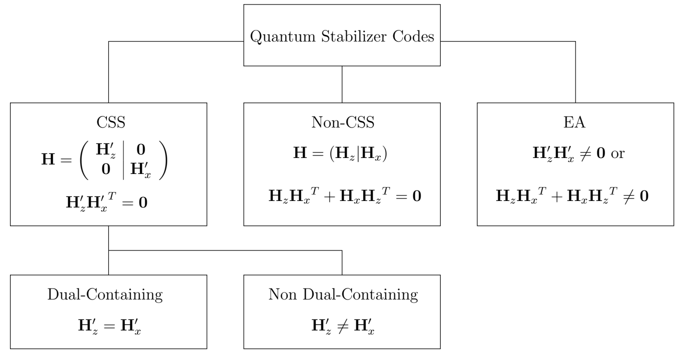

Fig. 3: The classification and characterization of QSCs, where CSS stands for *Calderbank-Shor-Steane* and EA for *entanglement assisted*.

IV. Protecting A Single Qubit: Design Examples

In Section I, we have already mentioned the three pioneering contributions on QSCs, which are only capable of handling a single qubit error, while in Section III, we briefly highlighted the different types of QSC constructions. In this section, we will link up both ideas in a more concrete context.

A. *Classical and Quantum* $1/3$*-rate Repetition Codes*

Before we delve deeper into the aforementioned QSCs, let us commence with a simple $1/3$-rate classical repetition codes, which maps a binary digit of "0" or "1" into a vector that contains three replicas of each binary digit as

$$0 \xrightarrow{\mathbf{G}} \begin{pmatrix} 0 & 0 & 0 \end{pmatrix},$$
$$1 \xrightarrow{\mathbf{G}} \begin{pmatrix} 1 & 1 & 1 \end{pmatrix}. \tag{19}$$

In classical codes, the mapping of information words into codewords may be described using the generator matrix $\mathbf{G}$ as encapsulated below:

$$\mathbf{y} = \mathbf{x} * \mathbf{G}, \tag{20}$$

where $\mathbf{y}$ denotes the vector of an n-bit codeword, $\mathbf{x}$ is the k-bit original information word and $*$ represents the matrix multiplication over modulo-2. Hence, the generator matrix $\mathbf{G}$ is a $(k \times n)$-element matrix, which may be decomposed into a systematic form as

$$\mathbf{G} = (\mathbf{I}_k|\mathbf{P}), \tag{21}$$

where $\mathbf{I}_k$ is a $(k \times k)$ identity matrix and $\mathbf{P}$ is a $k \times (n-k)$-element matrix. The form given in Eq. (21) represents systematic linear block codes since, the codeword consists of k-bit information word followed by $(n-k)$ parity bits. Each generator matrix $\mathbf{G}$ corresponds to an $(n-k) \times n$-element PCM $\mathbf{H}$, which is defined as

$$\mathbf{H} = \left(\mathbf{P}^T|\mathbf{I}_{n-k}\right). \tag{22}$$

The PCM of $\mathbf{H}$ is constructed for ensuring that $\mathbf{y}$ is a valid codeword if and only if

$$\mathbf{y} * \mathbf{H}^T = \mathbf{0}. \tag{23}$$

A received word $\widehat{\mathbf{y}}$ may be contaminated by an error vector $\mathbf{e}$ due to the channel impairments, so that $\widehat{\mathbf{y}} = \mathbf{y} + \mathbf{e}$. The error

[3]The dual pair of the linear binary code $C_1 \subset \mathbb{F}_2^n$ is defined by a linear binary code $C_2 = \{c_2 \in \mathbb{F}_2^n | \langle c_1, c_2 \rangle = 0, \forall c_1 \in \mathcal{C}_1\}$, where $\langle c_1, c_2 \rangle$ represents the inner product between c_1 and c_2.

syndrome $\mathbf{s}$ is a vector of length $(n-k)$ that is obtained by following calculation:

$$\begin{aligned}\mathbf{s} = \widehat{\mathbf{y}} * \mathbf{H}^T &= (\mathbf{y}+\mathbf{e}) * \mathbf{H}^T \\ &= \mathbf{y} * \mathbf{H}^T + \mathbf{e} * \mathbf{H}^T \\ &= \mathbf{0} + \mathbf{e} * \mathbf{H}^T \\ &= \mathbf{e} * \mathbf{H}^T. \end{aligned} \tag{24}$$

In simple terms, we have 2^k legitimate codewords representing k information bits, 2^n possible received bit patterns of $\widehat{\mathbf{y}}$, and $2^{(n-k)}$ syndromes of $\mathbf{s}$ each unambiguously identifying one of the $2^{(n-k)}$ error patterns, including the error-free scenario.

Hence, from this brief description of basic classical codes, the mapping in Eq. (19) can be encapsulated into a generator matrix $\mathbf{G}$ as given below:

$$\mathbf{G} = \begin{pmatrix}1 & 1 & 1\end{pmatrix}. \tag{25}$$

From the generator matrix $\mathbf{G}$ given in Eq. (25) and the PCM formulation given in Eq. (21), we obtain the PCM $\mathbf{H}$ for a $1/3$-rate classical repetition code encapsulated by

$$\mathbf{H} = \begin{pmatrix}1 & 1 & 0\\ 1 & 0 & 1\end{pmatrix}, \tag{26}$$

where the first row returns the first bit of the two bits syndrome value and acccordingly the second row evaluates the second bit. Thus, it can be easily checked by using the syndrome computation of Eq. (24) that the syndrome value of $(0\ 0)$ is obtained if the received word $\widehat{\mathbf{y}}$ is equal to the valid codeword, either $(0\ 0\ 0)$ or $(1\ 1\ 1)$. The syndrome computation yields a syndrome vector with $(n-k)$-element and in this case for a $1/3$-rate classical repetition code, it generates a synfrome vector with two elements. Therefore, there are four possible outcomes from the syndrome computation and one of them indicates the error-free received word, which is the $(0\ 0)$ syndrome. Since a $1/3$-rate classical repetition code is considered as a short block code, the syndrome computation and the associated error pattern is readily checked using a look-up table, namely Table. I.

TABLE I: Syndrome computation and the associated error pattern for a $1/3$-rate classical repetition code.

Syndrome ($\mathbf{s}$)	Error Pattern ($\mathbf{e}$)	Index of Corrupted Bit
$(0\ 0)$	$(0\ 0\ 0)$	-
$(0\ 1)$	$(0\ 0\ 1)$	3
$(1\ 0)$	$(0\ 1\ 0)$	2
$(1\ 1)$	$(1\ 0\ 0)$	1

Next, we proceed with with a simple $1/3$-rate quantum repetition code that capable of recovering a bit-flip error. Let us assume that we have a quantum state $|\psi\rangle = \alpha_0|0\rangle + \alpha_1|1\rangle$. As the consequence of the *No Cloning Theorem* of quantum mechanics, there is no unitary transformation U capable of mapping an arbitrary quantum state $|\psi\rangle$ onto a state of $|\overline{\psi}\rangle = |\psi\rangle^{\otimes 3}$. Hence, the code mapping of quantum state $|0\rangle$ and $|1\rangle$ by a unitary transformation U is defined by

$$\begin{aligned}|0\rangle &\rightarrow |000\rangle,\\ |1\rangle &\rightarrow |111\rangle.\end{aligned} \tag{27}$$

In a more general scenario, the mapping of k logical qubits to n physical qubits is encapsulated as follows:

$$|\psi\rangle \otimes |0\rangle^{\otimes(n-k)} \xrightarrow{U} |\overline{\psi}\rangle = \alpha_0|0\rangle_L + \alpha_1|1\rangle_L, \tag{28}$$

where $|0\rangle_L$ denotes the encoded state of the logical qubit $|0\rangle$, $|1\rangle_L$ denotes the encoded state of logical qubit $|1\rangle$, while $|0\rangle^{\otimes n-k}$ represents the auxiliary or the redundant qubits (*ancillas*), and the superscript of $\otimes(n-k)$ represents $(n-k)$-fold of tensor products. Hence, for $1/3$-rate quantum repetition codes, the state of the logical qubit $|\psi\rangle$ corresponds to the state of the physical qubit $|\overline{\psi}\rangle$ as given by

$$(\alpha_0|0\rangle + \alpha_1|1\rangle) \otimes |0\rangle^{\otimes 2} \xrightarrow{U} |\overline{\psi}\rangle = \alpha_0|000\rangle + \alpha_1|111\rangle, \tag{29}$$

where the $|000\rangle$ defines the encoded logical qubit $|0\rangle_L$ and $|111\rangle$ defines the $|1\rangle_L$. Again, it is important to bear in mind that the state of $|\overline{\psi}\rangle = \alpha_0|000\rangle + \alpha_1|111\rangle$ is not equal to $|\overline{\psi}\rangle = |\psi\rangle^{\otimes 3}$. More explicitly, this relationship can also be expressed as $|\overline{\psi}\rangle = \alpha_0|000\rangle + \alpha_1|111\rangle \neq |\psi\rangle^{\otimes 3}$. The state of the physical qubits of the $1/3$-rate quantum repetition code is stabilized, or synonymously 'parity-checked' by the pair of stabilizer operators $g_1 = \mathbf{ZZI}$ and $g_2 = \mathbf{ZIZ}$. A valid codeword or a valid encoded state, which is not affected by the stabilizer operators g_1 and g_2, has an input state of $|\overline{\psi}\rangle$ and returns the state of $|\overline{\psi}\rangle$, hence it yields the so-called eigenvalues of $+1$, and more explicitly, it is described below:

$$\begin{aligned}g_1|\overline{\psi}\rangle &= \alpha_0|000\rangle + \alpha_1|111\rangle \equiv |\overline{\psi}\rangle,\\ g_2|\overline{\psi}\rangle &= \alpha_0|000\rangle + \alpha_1|111\rangle \equiv |\overline{\psi}\rangle.\end{aligned} \tag{30}$$

By contrast, if the stabilizer operators g_1 and g_2 are applied to the corrupted states $|\widehat{\psi}\rangle$, they both yield eigenvalues that are not in the all one state. For instance, let us assume that we received a corrupted state having a bit-flip error imposed on the first qubit of $|\overline{\psi}\rangle$ yielding $|\widehat{\psi}\rangle = \alpha_0|100\rangle + \alpha_1|011\rangle$. Then, upon applying the stabilizer operators $g_1 = \mathbf{ZZI}$ and $g_2 = \mathbf{ZIZ}$ to the state of $|\widehat{\psi}\rangle$, it may be readily showed after few steps that we arrive at the following eigenvalues:

$$\begin{aligned}
g_1|\widehat{\psi}\rangle &= \mathbf{ZZI}(\alpha_0|100\rangle + \alpha_1|011\rangle) \\
&= \begin{pmatrix} 1 & 0 & 0 & 0 & 0 & 0 & 0 & 0 \\ 0 & 1 & 0 & 0 & 0 & 0 & 0 & 0 \\ 0 & 0 & -1 & 0 & 0 & 0 & 0 & 0 \\ 0 & 0 & 0 & -1 & 0 & 0 & 0 & 0 \\ 0 & 0 & 0 & 0 & -1 & 0 & 0 & 0 \\ 0 & 0 & 0 & 0 & 0 & -1 & 0 & 0 \\ 0 & 0 & 0 & 0 & 0 & 0 & 1 & 0 \\ 0 & 0 & 0 & 0 & 0 & 0 & 0 & 1 \end{pmatrix} \cdot \begin{pmatrix} 0 \\ 0 \\ 0 \\ \alpha_1 \\ \alpha_0 \\ 0 \\ 0 \\ 0 \end{pmatrix} \\
&= \begin{pmatrix} 0 \\ 0 \\ 0 \\ -\alpha_1 \\ -\alpha_0 \\ 0 \\ 0 \\ 0 \end{pmatrix} \equiv -\alpha_0|100\rangle - \alpha_1|011\rangle \equiv -|\widehat{\psi}\rangle, \qquad (31)
\end{aligned}$$

$$\begin{aligned}
g_2|\widehat{\psi}\rangle &= \mathbf{ZIZ}(\alpha_0|100\rangle + \alpha_1|011\rangle) \\
&= \begin{pmatrix} 1 & 0 & 0 & 0 & 0 & 0 & 0 & 0 \\ 0 & -1 & 0 & 0 & 0 & 0 & 0 & 0 \\ 0 & 0 & 1 & 0 & 0 & 0 & 0 & 0 \\ 0 & 0 & 0 & -1 & 0 & 0 & 0 & 0 \\ 0 & 0 & 0 & 0 & -1 & 0 & 0 & 0 \\ 0 & 0 & 0 & 0 & 0 & 1 & 0 & 0 \\ 0 & 0 & 0 & 0 & 0 & 0 & -1 & 0 \\ 0 & 0 & 0 & 0 & 0 & 0 & 0 & 1 \end{pmatrix} \cdot \begin{pmatrix} 0 \\ 0 \\ 0 \\ \alpha_1 \\ \alpha_0 \\ 0 \\ 0 \\ 0 \end{pmatrix} \\
&= \begin{pmatrix} 0 \\ 0 \\ 0 \\ -\alpha_1 \\ -\alpha_0 \\ 0 \\ 0 \\ 0 \end{pmatrix} \equiv -\alpha_0|100\rangle - \alpha_1|011\rangle \equiv -|\widehat{\psi}\rangle. \qquad (32)
\end{aligned}$$

The resultant eigenvalues of ± 1 act similarly to the syndrome vector of classical codes, where the eigenvalue $+1$ is associated with the classical syndrome value 0 and the eigenvalue -1 with the classical syndrome value 1. More explicitly, the single qubit error patterns imposed on the $1/3$-rate quantum repetition codes and the associated eigenvalues are portrayed in Table. II. However, this specific construcion is only capable of detecting and correcting a single bit-flip error imposed by the Pauli channel on the physical qubits, but no phase-flips.

Since the physical qubits may experience not only bit-flip errors, but also phase-flip errors as well as both bit-flip and phase-flip errors, different mapping is necessitated to protect the physical qubits from phase-flip error. In order to protect the physical qubits from a phase-flip error, we may require a different basis but we can still invoke a similar approach. To elaborate further, the Hadamard transformation ($\mathbf{H}$) maps the computational basis of $\{|0\rangle, |1\rangle\}$ onto the Hadamard basis of $\{|+\rangle, |-\rangle\}$, where the state of $|+\rangle$ and $|-\rangle$ are defined as

$$|+\rangle \equiv \mathbf{H}|0\rangle = \frac{1}{\sqrt{2}}(|0\rangle + |1\rangle), \qquad (33)$$

$$|-\rangle \equiv \mathbf{H}|1\rangle = \frac{1}{\sqrt{2}}(|0\rangle - |1\rangle), \qquad (34)$$

and the unitary Hadamard transformation $\mathbf{H}$, which acts on a single qubit state, is given by

$$\mathbf{H} = \frac{1}{\sqrt{2}} \begin{pmatrix} 1 & 1 \\ 1 & -1 \end{pmatrix}. \qquad (35)$$

A phase-flip error defined over the Hadamard basis of $\{|+\rangle, |-\rangle\}$ acts similarly to the bit-flip error defined over the computational basis of $\{|0\rangle, |1\rangle\}$. Hence, for handling of a single phase-flip error, the code mapping of $1/3$-rate quantum repetition codes are given by

$$\begin{aligned} |0\rangle &\rightarrow |+++\rangle, \\ |1\rangle &\rightarrow |---\rangle. \end{aligned} \qquad (36)$$

Hence, the logical qubit of $|\psi\rangle$ corresponding to the physical qubits $|\overline{\psi}\rangle$ is given by

$$|\psi\rangle \otimes |0\rangle^{\otimes 2} \xrightarrow{U} |\overline{\psi}\rangle = \alpha_0|+++\rangle + \alpha_1|---\rangle. \qquad (37)$$

The state of physical qubits given in Eq. (37) can be stabilized by the operators $g_1 = \mathbf{XXI}$ and $g_2 = \mathbf{XIX}$. The detection and correction of a phase flip error can be carried out in analogy with the $1/3$-rate quantum repetition code for handling the bit-flip error.

As seen in Eq. (16), the stabilizer operators can be derived from the classical PCM $\mathbf{H}$ by mapping the Pauli matrices $\mathbf{I}$, $\mathbf{X}$, $\mathbf{Y}$ and $\mathbf{Z}$ onto $(\mathbb{F}_2)^2$ as follows:

$$\begin{aligned} \mathbf{I} &\rightarrow \left(0 \mid 0 \right), \\ \mathbf{X} &\rightarrow \left(0 \mid 1 \right), \\ \mathbf{Y} &\rightarrow \left(1 \mid 1 \right), \\ \mathbf{Z} &\rightarrow \left(1 \mid 0 \right). \end{aligned} \qquad (38)$$

Each row of $\mathbf{H}$ is associated with a stabilizer operator $g_i \in \mathcal{H}$, where the i-th column of both $\mathbf{H}_z$ and $\mathbf{H}_x$ corresponds to the i-th qubit and the binary 1 locations represent the $\mathbf{Z}$ and $\mathbf{X}$ positions in the PCMs $\mathbf{H}_z$ and $\mathbf{H}_x$, respectively. For instance, for the $1/3$-rate quantum repetition code, which is stabilized by the operators $g_1 = \mathbf{ZZI}$ and $g_2 = \mathbf{ZIZ}$, the PCM $\mathbf{H}$ is given as follows:

$$\mathbf{H} = \left(\begin{array}{ccc|ccc} 1 & 1 & 0 & 0 & 0 & 0 \\ 1 & 0 & 1 & 0 & 0 & 0 \end{array} \right). \qquad (39)$$

Since the $1/3$-rate quantum repetition code in this example can only correct a bit-flip ($\mathbf{X}$) error, which is stabilized by the $\mathbf{Z}$ operators, the PCM $\mathbf{H}_x$ contains only zero elements. The same goes for a $1/3$-rate quantum repetition code conceived for handling a phase-flip ($\mathbf{Z}$) error, which is stabilized by the operators $g_1 = \mathbf{XXI}$ and $g_2 = \mathbf{XIX}$. The PCM $\mathbf{H}$ corresponding to this particular QSC is defined as follows:

$$\mathbf{H} = \left(\begin{array}{ccc|ccc} 0 & 0 & 0 & 1 & 1 & 0 \\ 0 & 0 & 0 & 1 & 0 & 1 \end{array} \right). \qquad (40)$$

TABLE II: Single qubit bit-flip errors along with the associated eigenvalues in $1/3$-rate quantum repetition where the eigenvalues act similarly with the syndrome values in classical linear block codes.

Received States ($\|\widehat{\psi}\rangle$)	Eigenvalue $g_1\|\widehat{\psi}\rangle$	Eigenvalue $g_2\|\widehat{\psi}\rangle$	Syndrome ($\mathbf{s}$)	Index of Corrupted Qubit
$\alpha_0\|000\rangle + \alpha_1\|111\rangle$	$+1$	$+1$	(0 0)	-
$\alpha_0\|001\rangle + \alpha_1\|110\rangle$	$+1$	-1	(0 1)	3
$\alpha_0\|010\rangle + \alpha_1\|101\rangle$	-1	$+1$	(1 0)	2
$\alpha_0\|100\rangle + \alpha_1\|011\rangle$	-1	-1	(1 1)	1

It is clearly shown in Eq. (39) and (40) that the PCM of a $1/3$-rate quantum repetition code is similar to that of the $1/3$-rate classical repetition code given in Eq. (26).

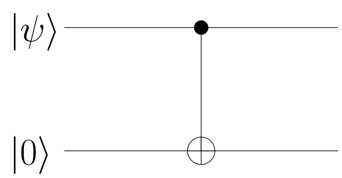

Fig. 4: The circuit representation of the CNOT unitary transformation.

In order to encode the logical qubits into physical qubits, we require the unitary transformation U acting as the quantum encoding circuit. To represent the quantum encoding circuit, one of the essential components is the controlled-NOT (CNOT) quantum gate. A CNOT quantum gate manipulates the state of a two-qubit system and it can be represented by a unitary transformation as follows:

$$\mathbf{CNOT} = \begin{pmatrix} 1 & 0 & 0 & 0 \\ 0 & 1 & 0 & 0 \\ 0 & 0 & 0 & 1 \\ 0 & 0 & 1 & 0 \end{pmatrix}. \tag{41}$$

The circuit representation of the CNOT quantum gate is depicted in Fig 4, which manipulates the state of two qubits and it can be formulated as follows:

$$\mathbf{CNOT}(|a_0, a_1\rangle) \equiv |a_0, (a_0 \oplus a_1)\rangle, \tag{42}$$

where the notation of $\oplus$ represents the modulo-2 addition. For instance, by using the CNOT representation in Eq. (41), a logical qubit in the superimposed state of $|\psi\rangle = \alpha_0|0\rangle + \alpha_1|1\rangle$ and a qubit in the pure state of $|0\rangle$ are manipulated by the quantum CNOT gate into following state:

$$\begin{aligned} \mathbf{CNOT}(|\psi\rangle, |0\rangle) &= \mathbf{CNOT}(\alpha_0|0\rangle + \alpha_1|1\rangle, |0\rangle) \\ &= \mathbf{CNOT}(\alpha_0|00\rangle + \alpha_1|10\rangle) \\ &= \begin{pmatrix} 1 & 0 & 0 & 0 \\ 0 & 1 & 0 & 0 \\ 0 & 0 & 0 & 1 \\ 0 & 0 & 1 & 0 \end{pmatrix} \cdot \begin{pmatrix} \alpha_{00} \\ 0 \\ \alpha_{10} \\ 0 \end{pmatrix} \\ &= \begin{pmatrix} \alpha_0 \\ 0 \\ 0 \\ \alpha_1 \end{pmatrix} \equiv \alpha_0|00\rangle + \alpha_1|11\rangle. \end{aligned} \tag{43}$$

Similarly, we may also use the CNOT definition given in Eq. (42) to determine the resultant state as described below:

$$\begin{aligned} \mathbf{CNOT}(|\psi\rangle, |0\rangle) &= \mathbf{CNOT}(\alpha_0|0\rangle + \alpha_1|1\rangle, |0\rangle) \\ &= \mathbf{CNOT}(\alpha_0|00\rangle + \alpha_1|10\rangle) \\ &= \alpha_0|0, (0 \oplus 0)\rangle + \alpha_1|1, (1 \oplus 0)\rangle \\ &= \alpha_0|00\rangle + \alpha_1|11\rangle. \end{aligned} \tag{44}$$

In this configuration, the first qubit is referred to as the *control qubit*, while the second one is referred to as the *target qubit*. The value of the target qubit is flipped if the value of the control qubit is equal to "1". We can observe that the CNOT quantum gate behaves similarly to the exclusive OR (XOR) gate of the classical computer.

For the sake of creating the encoded state of $1/3$-rate quantum repetition code, we require a single logical qubit and two ancillas prepared in the pure state of $|0\rangle$, as described in Eq. (29). In the first step, the CNOT unitary transformation is performed between the logical qubit and the first ancilla, in which the logical qubit acts as the control qubit and the ancilla as the target qubit. The same step is repeated during the second stage between the logical qubit and the second ancilla, where the second ancilla is also preserved as the target qubit. Therefore, the encoding circuit of the $1/3$-rate quantum repetition code can be represented as in Fig 5, which was designed for protecting the physical qubits from a single bit-flip error, as also seen in the mapping given in Eq. (27). For its $1/3$-rate quantum repetition code counterpart protecting the physical qubits from a phase-flip error, we require the Hadamard transformation to obtain the mapping given in Eq. (36). Hence, we can readily create the encoding circuit for a $1/3$-rate quantum repetition code for protecting the physical qubits from a phase-flip error by placing the Hadamard transformations after the second stage as portrayed in Fig. 6.

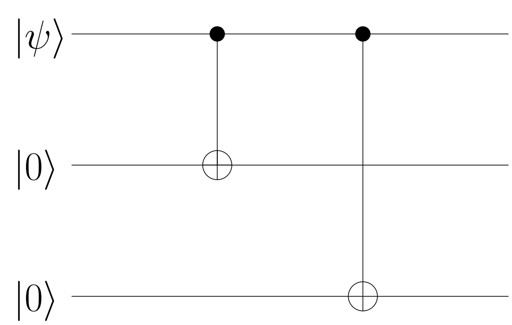

Fig. 5: The encoding circuit of the $1/3$-rate quantum repetition code protecting the physical qubits from a bit-flip error.

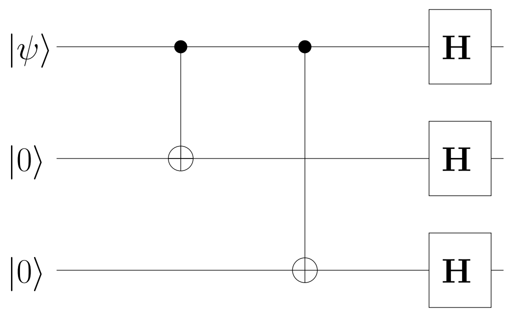

Fig. 6: The encoding circuit of the $1/3$-rate quantum repetition code protecting the physical qubits from a phase-flip error.

B. Shor's 9-Qubit Code

Since, we have elaborated briefly on the construction of QSCs along with the Pauli to binary isomorphism, we may now proceed with the corresponding examples of different QSC constructions conceived for protecting the physical qubits from any type of a single qubit error. Firstly, we start with the Shor's code [16]. In order to protect the qubits from any type of single qubit error, a logical qubit is mapped onto nine physical qubits. This code may also be viewed as a concatenated version of two $1/3$-rate quantum repetition codes, where the first stage is dedicated to the protection of the physical qubits from phase-flip errors, while the second stage is invoked for handling the bit-flip errors. To elaborate further, at the first stage of Shor's code, the state of a logical qubit is encoded by using the following mapping: $|0\rangle \rightarrow |+++\rangle$, $|1\rangle \rightarrow |---\rangle$. At the second stage, we encode each of the states of $|+\rangle$ to the state of $(|000\rangle + |111\rangle)/\sqrt{2}$, while the state of $|-\rangle$ is mapped to the state of $(|000\rangle - |111\rangle)/\sqrt{2}$. Therefore, the final state of the encoded logical qubits $|0\rangle_L$ and $|1\rangle_L$ are encapsulated as follows:

$$\begin{aligned}|0\rangle_L =& \frac{1}{\sqrt{2}}(|000\rangle + |111\rangle) \otimes \frac{1}{\sqrt{2}}(|000\rangle + |111\rangle)\\ &\otimes \frac{1}{\sqrt{2}}(|000\rangle + |111\rangle)\\ =& \frac{1}{2\sqrt{2}}(|000000000\rangle + |000000111\rangle + |000111000\rangle\\ &+ |000111111\rangle + |111000000\rangle + |111000111\rangle\\ &+ |111111000\rangle + |111111111\rangle), \end{aligned} \tag{45}$$

$$\begin{aligned}|1\rangle_L =& \frac{1}{\sqrt{2}}(|000\rangle - |111\rangle) \otimes \frac{1}{\sqrt{2}}(|000\rangle - |111\rangle)\\ &\otimes \frac{1}{\sqrt{2}}(|000\rangle - |111\rangle)\\ =& \frac{1}{2\sqrt{2}}(|000000000\rangle - |000000111\rangle - |000111000\rangle\\ &+ |000111111\rangle - |111000000\rangle + |111000111\rangle\\ &+ |111111000\rangle - |111111111\rangle). \end{aligned} \tag{46}$$

Based on the given description, the encoding circuit of Shor's code is portrayed in Fig. 7. The state determined by the nine physical qubits of Shor's code, where the latter defined in Eq. (45) and (46), is stabilized by the eight stabilizer operators which are listed in Table III.

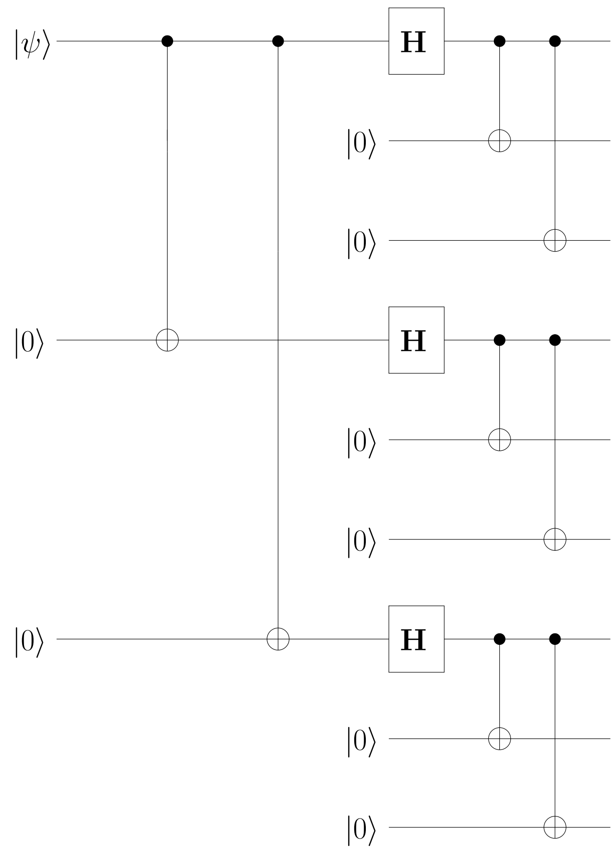

Fig. 7: The encoding circuit of Shor's 9-qubit code.

TABLE III: The eight stabilizer operators g_1 to g_8 of Shor's 9-qubit code, which stabilizes a single logical qubit with the aid of eight auxiliarry qubits.

g_i	Stabilizer Operator
g_1	**ZZIIIIIII**
g_2	**IZZIIIIII**
g_3	**IIIZZIIII**
g_4	**IIIIZZIII**
g_5	**IIIIIIZZI**
g_6	**IIIIIIIZZ**
g_7	**XXXXXXIII**
g_8	**IIIXXXXXX**

To elaborate a little further, Shor's code is a member of the class of non-dual-containing CSS codes. Explicitly, it belongs to the class of CSS codes because the stabilizer formalism of Shor's code implies that the code handles the $\mathbf{Z}$ error and the $\mathbf{X}$ error separately, whilst it is a non-dual-containing because the PCMs $\mathbf{H}_z$ and $\mathbf{H}_x$ are not identical. Based on the list of stabilizer operators given in Table III, the PCM $\mathbf{H}$ of Shor's code is given in Eq. (45), where each row of the PCM corresponds to each of the stabilizer operators listed in Table III. The quantum coding rate (r_Q) of a quantum code $\mathcal{C}[n, k]$ is defined by the ratio of the number of logical qubits k to the number of physical qubits n, which can be formulated as

$$r_Q = \frac{k}{n}. \tag{46}$$

$$
\mathbf{H}_{Shor} = \left(\begin{array}{ccccccccc|ccccccccc}
1 & 1 & 0 & 0 & 0 & 0 & 0 & 0 & 0 & 0 & 0 & 0 & 0 & 0 & 0 & 0 & 0 & 0 \\
0 & 1 & 1 & 0 & 0 & 0 & 0 & 0 & 0 & 0 & 0 & 0 & 0 & 0 & 0 & 0 & 0 & 0 \\
0 & 0 & 0 & 1 & 1 & 0 & 0 & 0 & 0 & 0 & 0 & 0 & 0 & 0 & 0 & 0 & 0 & 0 \\
0 & 0 & 0 & 0 & 1 & 1 & 0 & 0 & 0 & 0 & 0 & 0 & 0 & 0 & 0 & 0 & 0 & 0 \\
0 & 0 & 0 & 0 & 0 & 0 & 1 & 1 & 0 & 0 & 0 & 0 & 0 & 0 & 0 & 0 & 0 & 0 \\
0 & 0 & 0 & 0 & 0 & 0 & 0 & 1 & 1 & 0 & 0 & 0 & 0 & 0 & 0 & 0 & 0 & 0 \\
0 & 0 & 0 & 0 & 0 & 0 & 0 & 0 & 0 & 1 & 1 & 1 & 1 & 1 & 1 & 0 & 0 & 0 \\
0 & 0 & 0 & 0 & 0 & 0 & 0 & 0 & 0 & 0 & 0 & 0 & 1 & 1 & 1 & 1 & 1 & 1
\end{array}\right). \tag{45}
$$

Hence again, for a Shor's 9-qubit code the quantum coding rate is $r_Q = 1/9$.

C. Steane's 7-Qubit Code

Steane's code was proposed to protect a single qubit from any type of error by mapping a logical qubit onto seven physical qubits, instead of nine qubits. In contrast to Shor's code, Steane's code is a dual-containing CSS code, since the PCMs $\mathbf{H}_z$ and $\mathbf{H}_x$ are equal to that of clasical Hamming code $\mathbf{H}_{Ham}$, which is given by

$$
\mathbf{H}_{Ham} = \begin{pmatrix} 1 & 1 & 0 & 1 & 1 & 0 & 0 \\ 1 & 0 & 1 & 1 & 0 & 1 & 0 \\ 0 & 1 & 1 & 1 & 0 & 0 & 1 \end{pmatrix}. \tag{47}
$$

It can be confimed that the classical Hamming code is a dual-containing code, because it satisfies the condition $\mathbf{H}_{Ham}.\mathbf{H}_{Ham}^T = 0$. Therefore, the PCM $\mathbf{H}$ of Steane's code is defined as shown in Eq. (48).

Since Steane's code is a member of the dual-containing CSS codes, the encoded state of the logical qubit $|0\rangle_L$ and $|1\rangle_L$ may be determined from its classical code counterpart. Let $\mathcal{C}_1(7,4)$ be the Hamming code and $\mathcal{C}_2(7,3)$ be its dual. Both of the codes are capable of corrrecting one bit error. Hence, the resultant CSS quantum code derived from these codes, namely the $\mathcal{C}[n, k_1 - k_2] = \mathcal{C}[7,1]$, also capable of correcting a single qubit error. For Steane's code the states of encoded logical qubit of $|0\rangle_L$ and $|1\rangle_L$ are defined as follows:

$$
|0\rangle_L = \frac{1}{\sqrt{|\mathcal{C}_2|}} \sum_{x \in \mathcal{C}_1, \mathcal{C}_2} |x\rangle, \tag{49}
$$

$$
|1\rangle_L = \frac{1}{\sqrt{|\mathcal{C}_2|}} \sum_{x \in \mathcal{C}_1, x \notin \mathcal{C}_2} |x\rangle. \tag{50}
$$

Since $\mathcal{C}_2$ is the dual of $\mathcal{C}_1$, by definition the PCM of $\mathcal{C}_2$, denoted by $\mathbf{H}(\mathcal{C}_2)$ is the generator matrix of $\mathcal{C}_1$, denoted by $\mathbf{G}(\mathcal{C}_1)$. Hence, the parity-check matrix of $\mathcal{C}_2$ can be written as

$$
\mathbf{H}(\mathcal{C}_2) = \mathbf{G}(\mathcal{C}_1) = \begin{pmatrix} 1 & 0 & 0 & 0 & 1 & 1 & 0 \\ 0 & 1 & 0 & 0 & 1 & 0 & 1 \\ 0 & 0 & 1 & 0 & 0 & 1 & 1 \\ 0 & 0 & 0 & 1 & 1 & 1 & 1 \end{pmatrix}. \tag{51}
$$

Based on the PCM given in Eq. (47) and (51), we can define the code space of $\mathcal{C}_1$ and $\mathcal{C}_2$, which is described in Table IV. Finally, using Eq. (49), (50), and also the code space given in Table IV, the encoded states of the logical qubit $|0\rangle_L$ and $|1\rangle_L$ of the Steane's code are as follows:

TABLE IV: The code space of $\mathcal{C}_1$ and $\mathcal{C}_2$ for determining the encoded state of the Steane's code.

$x \in \mathcal{C}_1, \mathcal{C}_2$	$x \in \mathcal{C}_1, x \notin \mathcal{C}_2$
0000000	1111111
0111001	1000110
1011010	0100101
1100011	0011100
1101100	0010011
1010101	0101010
0110110	1001001
0001111	1110000

$$
\begin{aligned}
|0\rangle_L = \frac{1}{2\sqrt{2}}(&|00000000\rangle + |0111001\rangle + |1011010\rangle \\
&+ |1100011\rangle + |1101100\rangle + |1010101\rangle \\
&+ |0110110\rangle + |0001111\rangle),
\end{aligned} \tag{52}
$$

$$
\begin{aligned}
|1\rangle_L = \frac{1}{2\sqrt{2}}(&|1111111\rangle + |1000110\rangle + |0100101\rangle \\
&+ |0011100\rangle + |0010011\rangle + |0101010\rangle \\
&+ |1001001\rangle + |1110000\rangle).
\end{aligned} \tag{53}
$$

It can be readily seen that the quantum coding rate of Steane's 7-qubit code is $1/7$. The encoding circuit of the Steane's $1/7$-rate code can be found in [72].

TABLE V: The stabilizer formalism of the Steane's 7-qubit code.

g_i	Stabilizer Operator
g_1	**ZZIZZII**
g_2	**ZIZZIZI**
g_3	**IZZZIIZ**
g_4	**XXIXXII**
g_5	**XIXXIXI**
g_6	**IXXXIIX**

D. Laflamme's 5-Qubit Code - The Perfect Code

Laflamme's code maps a single logical qubit onto a five physical qubits. Laflamme's code is also referred to as the "perfect code", because it has been proven that in order to protect a logical qubit, the lowest number of physical qubits required is five [19], [20]. The perfect 5-qubit code is a non-CSS code, since the stabilizer formalism is designed to handle

$$\mathbf{H}_{Steane} = \left(\begin{array}{c|c} \mathbf{H}_{Ham} & \mathbf{0} \\ \mathbf{0} & \mathbf{H}_{Ham} \end{array} \right) = \left(\begin{array}{ccccccc|ccccccc} 1 & 1 & 0 & 1 & 1 & 0 & 0 & 0 & 0 & 0 & 0 & 0 & 0 & 0 \\ 1 & 0 & 1 & 1 & 0 & 1 & 0 & 0 & 0 & 0 & 0 & 0 & 0 & 0 \\ 0 & 1 & 1 & 1 & 0 & 0 & 1 & 0 & 0 & 0 & 0 & 0 & 0 & 0 \\ 0 & 0 & 0 & 0 & 0 & 0 & 0 & 1 & 1 & 0 & 1 & 1 & 0 & 0 \\ 0 & 0 & 0 & 0 & 0 & 0 & 0 & 1 & 0 & 1 & 1 & 0 & 1 & 0 \\ 0 & 0 & 0 & 0 & 0 & 0 & 0 & 0 & 1 & 1 & 1 & 0 & 0 & 1 \end{array} \right). \tag{48}$$

the $\mathbf{Z}$ errors and $\mathbf{X}$ errors simultaneously. There are several existing designs related to the perfect 5-qubit code [18], [71] and in this treatise, we use the PCM formulation given in [71]. Explicitly, its non-CSS characteristics can be readily observed from the PCM $\mathbf{H}_{perfect}$ of the 5-qubit perfect code, which is specified as follows:

$$\mathbf{H}_{perfect} = \left(\begin{array}{ccccc|ccccc} 0 & 1 & 1 & 0 & 0 & 1 & 0 & 0 & 1 & 0 \\ 0 & 0 & 1 & 1 & 0 & 0 & 1 & 0 & 0 & 1 \\ 0 & 0 & 0 & 1 & 1 & 1 & 0 & 1 & 0 & 0 \\ 1 & 0 & 0 & 0 & 1 & 0 & 1 & 0 & 1 & 0 \end{array} \right). \tag{54}$$

TABLE VI: The stabilizer formalism of the perfect 5-qubit code.

g_i	Stabilizer Operator
g_1	**XZZXI**
g_2	**IXZZX**
g_3	**XIXZZ**
g_4	**ZXIXZ**

Hence, the stabilizer operators of the 5-qubit code may be explicitly formulated as in Table VI. In general, the states of encoded logical qubit of QSCs are defined as follows:

$$|0\rangle_L = \sum_{g_i \in \mathcal{S}} g_i |0\rangle^{\otimes N}, \tag{55}$$

$$|1\rangle_L = \overline{\mathbf{X}} |0\rangle_L. \tag{56}$$

TABLE VII: List of valid stabilizer operators for determining the encoded state of the 5-qubit code.

Stabilizer	State	Stabilizer	State
g_0	$\|00000\rangle$	g_2g_3	$-\|11101\rangle$
g_1	$\|10010\rangle$	g_2g_4	$-\|00011\rangle$
g_2	$\|01001\rangle$	g_3g_4	$-\|11110\rangle$
g_3	$\|10100\rangle$	$g_1g_2g_3$	$-\|01111\rangle$
g_4	$\|01010\rangle$	$g_1g_2g_4$	$-\|10001\rangle$
g_1g_2	$-\|11011\rangle$	$g_1g_3g_4$	$-\|01100\rangle$
g_1g_3	$-\|00110\rangle$	$g_2g_3g_4$	$-\|10111\rangle$
g_1g_4	$-\|11000\rangle$	$g_1g_2g_3g_4$	$\|00101\rangle$

The stabilizers $g_i \in \mathcal{S}$ includes all the valid stabilizer operators of the quantum code $\mathcal{C}$, which covers not only the stabilizer operators that are listed in Table VI. Because of the commutative property of the stabilizer formalism, the product of any two stabilizer operators generates another valid stabilizer operator. Table VII provides a list of all the possible combinations of the stabilizer operators, which includes the stabilizer operator of $g_0 = \mathbf{IIIII}$, and also the respective transformation upon the state of $|0\rangle^{\otimes 5} = |00000\rangle$. The notation of $\overline{\mathbf{X}}$ denotes the logical operator $\mathbf{X}$. Explicitly, in this case for the 5-qubit code the logical operator representing the encoded state of the logical qubit is $\overline{\mathbf{X}} = \mathbf{XXXXX}$. The logical operator is represented by an N-fold application of Pauli matrices that commutes with all stabilizer operators, but it is not a part of the set of valid stabilizer operators $\mathcal{S}$. The resultant quantum coding rate of the 5-qubit code is $r_Q = 1/5$. The encoded state mapping for the 5-qubit quantum code based on the Eq. (55), (56). Hence, the corresponding states, which are described in Table VII, are defined below:

$$\begin{aligned} |0\rangle_L = \frac{1}{4}(&|00000\rangle + |10010\rangle + |01001\rangle + |10100\rangle \\ &+ |01010\rangle - |11011\rangle - |00110\rangle - |11000\rangle \\ &- |11101\rangle - |00011\rangle - |11110\rangle - |01111\rangle \\ &- |10001\rangle - |01100\rangle - |10111\rangle + |00101\rangle), \end{aligned} \tag{57}$$

$$\begin{aligned} |1\rangle_L = \frac{1}{4}(&|11111\rangle + |01101\rangle + |10110\rangle + |01011\rangle \\ &+ |10101\rangle - |00100\rangle - |11001\rangle - |00111\rangle \\ &- |00010\rangle - |11100\rangle - |00001\rangle - |10000\rangle \\ &- |01110\rangle - |10011\rangle - |01000\rangle + |11010\rangle). \end{aligned} \tag{58}$$

The same method can be utilized for determining the encoded state of logical qubit for Shor's code and Steane's code. However, both Shor's code and Steane's code offer a more simplistic approach for determining their corresponding encoded states. The description for the efficient encoding circuit of the $1/5$-rate Laflamme's code can be found in [18], [73], [74].

Based on the aforementioned constructions, we evaluated the performance of the QSCs by simulation, in the context of quantum depolarizing channel. The performance of 9-qubit Shor's code, 7-qubit Steane's code and 5-qubit Laflamme's code are portrayed in Fig. 8 in terms of the qubit error rate (QBER) on given depolarizing probability (p). From the simulation result, it can be observed clearly that the performance of all three QSCs are quite similar. The similarity in performances are expected because all of the codes have the same error correction capability of correcting single qubit error. In addition, they utilize the hard decision decoding based on syndrome measurement. From this result, we may conclude that for different codes with the same error correction capability, where in classical coding theory it will be translated into the minimum distance property, they are associated with similar performances eventhough all of the codes have different codeword length. In this case, all of the QSCs have a

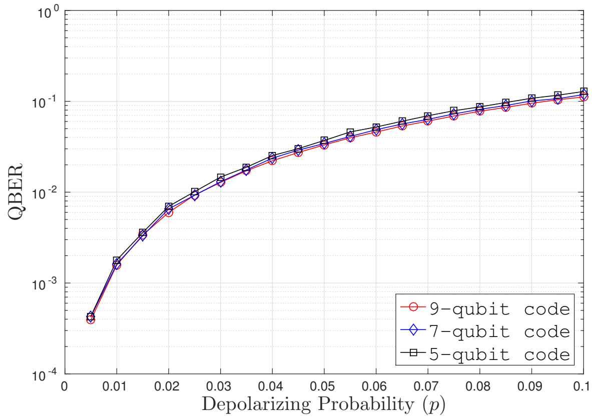

Fig. 8: QBER performance of the QSCs protecting a single qubit, namely Shor's 9-qubit code, Steane's 7-qubit code and the perfect 5-qubit code, recorded for the quantum depolarizing channel. The similarity of performances is due to the fact that all of the QSCs rely on hard-decision syndrome decoding and they all have the same error correction capabilities.

single qubit error correction capability ($t = 1$), and it may be translated as the minimum distance of three ($d = 3$), but having different codeword length, 9-qubit, 7-qubit and 5-qubit for Shor's code, Steane's code and Laflamme's code, respectively. Another fact that we should point out that the three codes exhibit different code constructions. Shor's code belongs to non dual-containing CSS codes, while Steane's code is a member of dual-containing CSS codes, and finally, Laflamme's code or the perfect 5-qubit code has a construction of non-CSS codes.

V. On Classical to Quantum Coding Bounds

In this section, we present the classical to quantum transformation of the most well-known coding bounds, namely the Singleton bound [75] and Hamming bound [76], which serve as the upper bounds, as well as the Gilbert-Varshamov (GV) bound [77], which acts as the lower bound. Although, there are several ways of deriving the coding bounds in the quantum domain, we are interested exploring the duality of coding bounds in classical and quantum domain. Therefore, we present the derivation of quantum coding bounds using the classical to quantum isomorphism approach and demonstrate that the final results agree with the coding bounds that are derived from a purely quantum domain perspective.

A. Singleton bound

The Singleton bound of classical binary code constructions $\mathcal{C}(n,k)$ is defined as

$$n - k \geq d - 1, \tag{59}$$

where the notation n denotes the codeword length, k for the length of information bits, and d for minimum distance amongst the codewords in codebook $\mathcal{C}$. Singleton bound acts as an upper bound in classical code constructions. The bound implies that the number of rows in a PCM associated with the length of syndrome vector, which is equal to $(n-k)$, has to be greater than $(d-1)$. For the QSC $\mathcal{C}[n,k]$, the rows of PCM correspond to the number stabilizer operators. Since the stabilizer formalism has to correct both the bit-flip errors and the phase-flip errors, the classical Singleton bound of Eq. (59) can be readily transformed into the quantum Singleton bound as follows:

$$n - k \geq 2(d-1), \tag{60}$$

where n now may also be referred to as the number of physical qubits and k as the number of logical qubits. In order to show explicitly the trade-off between the minimum distance and the quantum coding rate, Eq. (60) can be modified to

$$\frac{k}{n} \leq 1 - 2\left(\frac{d-1}{n}\right). \tag{61}$$

In the quantum domain, the Singleton bound is also known as the Knill-Laflamme bound [78]. The QSCs achieving the quantum Singleton bound by satisfying the equality are classified as the quantum Maximum Separable Distance (MDS) codes. One of the well-known QSCs having a minimum distance $d = 3$ that reaches the quantum Singleton bound is the perfect 5-qubit code $\mathcal{C}[n,k,d] = \mathcal{C}[5,1,3]$.

B. Hamming bound

In classical binary coding, a codebook $\mathcal{C}(n,k)$ maps the information words containing k bits into a codeword of length n bits. The maximal number of errors, which is denoted by t that can be corrected by codebook $\mathcal{C}$ is given by

$$t = \lfloor \frac{d-1}{2} \rfloor. \tag{62}$$

Therefore the maximum size of a binary codebook $|\mathcal{C}| = 2^k$ is bounded by the sphere-packing bound which is defined as:

$$2^k \leq \frac{2^n}{\sum_{j=0}^{t=\lfloor \frac{d-1}{2} \rfloor} \binom{n}{j}}. \tag{63}$$

Since the QSCs have to correct three different types of error namely the bit-flip errors ($\mathbf{X}$), phase-flip errors ($\mathbf{Z}$), as well as both bit-flip and phase-flip errors ($\mathbf{Y}$), the size of the codebook for a quantum code $\mathcal{C}[n,k]$ is now bounded by

$$2^k \leq \frac{2^n}{\sum_{j=0}^{t=\lfloor \frac{d-1}{2} \rfloor} \binom{n}{j} 3^j}. \tag{64}$$

By modifying Eq. (64), we can express explicitly the bound of the quantum coding rate as a function of the minimum distance d and codeword length n, as shown below:

$$\frac{k}{n} \leq 1 - \frac{1}{n} \log_2 \left(\sum_{j=0}^{t=\lfloor \frac{d-1}{2} \rfloor} \binom{n}{j} 3^j \right). \tag{65}$$

If n tends to ∞, we obtain

$$\frac{k}{n} \leq 1 - \left(\frac{d}{2n}\right) \log_2 3 - H\left(\frac{d}{2n}\right), \tag{66}$$

where $H(x)$ is the binary entropy of x formulated as $H(x) = -x\log_2 x - (1-x)\log_2(1-x)$. Equation (65) and (66) are also known as the quantum Hamming bound [20], which also constitutes the upper bound of quantum code constructions.

C. Gilbert-Varshamov bound

The same analogy exploited to derive the quantum Hamming bound may also be used for transforming the classical Gilbert-Varshamov (GV) bound, namely the lower bound for classical code constructions, into its quantum counterpart. In the classical domain, the GV bound is formulated as

$$2^k \geq \frac{2^n}{\sum_{j=0}^{d-1} \binom{n}{j}}. \tag{67}$$

Considering that the quantum codes have to tackle three different types of errors, the size of the codebook $\mathcal{C}[n,k]$ is bounded by

$$2^k \geq \frac{2^n}{\sum_{j=0}^{d-1} \binom{n}{j} 3^j}. \tag{68}$$

Hence, we can readily derive the quantum GV bound, the lower bound of the quantum coding rate as a function of the minimum distance d and codeword length n as follows:

$$\frac{k}{n} \geq 1 - \frac{1}{n}\log_2\left(\sum_{j=0}^{d-1}\binom{n}{j}3^j\right). \tag{69}$$

Again, if n aprroaches ∞, we obtain

$$\frac{k}{n} \geq 1 - \left(\frac{d}{n}\right)\log_2 3 - H\left(\frac{d}{n}\right), \tag{70}$$

where $H(x)$ is the binary entropy of x. The quantum GV bounds in Eq. (69) and (70) are valid for non-CSS QSCs. However, a special case should be considered for dual-containing quantum CSS codes. It will be shown in Section VII that for some dual-containing CSS codes the code constructions violate the quantum GV bound. Hence, a special bound has to be derived to accomodate the dual-containing CSS codes. In the classical domain, a binary code $\mathcal{C}(n,k)$ maps a k-bit information word into an n-bit encoded codeword. The number of syndrome measurement operators is determined by the number of rows in the parity-check matrix $\mathcal{C}(n,k)$, which is equal to $(n-k)$. With a simple modification of Eq. (67), the number of syndrome measurement operators in $\mathcal{C}(n,k)$ is bounded by

$$2^{(n-k)} \leq \left(\sum_{j=0}^{d-1}\binom{n}{j}\right). \tag{71}$$

Recall that the dual-containing quantum CSS codes rely on dual-containing classical binary codes, which satisfy the symplectic criterion of Eq. (17) and also comply with the constraint of $\mathbf{H}_z = \mathbf{H}_x$. Explicitly, half portion of the stabilizer operators of $\mathcal{C}[n,k]$ are mapped onto $\mathbf{H}_z$, while the other half are mapped onto $\mathbf{H}_x$. Therefore, the number of the stabilizer operators of a dual-containing quantum CSS code are bounded by

$$2^{\frac{(n-k)}{2}} \leq \left(\sum_{j=0}^{d-1}\binom{n}{j}\right). \tag{72}$$

Based on Eq. (72), we may formulate the lower bound on the quantum coding rate of a dual-containing quantum CSS code as follows:

$$\frac{k}{n} \geq 1 - \frac{2}{n}\log_2\left(\sum_{j=0}^{d-1}\binom{n}{j}\right). \tag{73}$$

As n approaches ∞, we obtain the quantum GV bound for CSS codes, as suggested in [66], which is formulated as

$$\frac{k}{n} \geq 1 - 2H\left(\frac{d}{n}\right), \tag{74}$$

where $H(x)$ is the binary entropy of x. Based on the discussions above, we compare the asymptotic classical and quantum coding bounds in Table. VIII as well as in Fig. 9. Since the QSCs are designed to mitigate both bit-flip errors as well as phase-flip errors, the bounds of QSCs are significantly lower than those of their classical counterparts. Nevertheless, the general conception still holds, the Singleton bound serves as the loose upper bound, whilst the Hamming bound is the tighter upper bound.

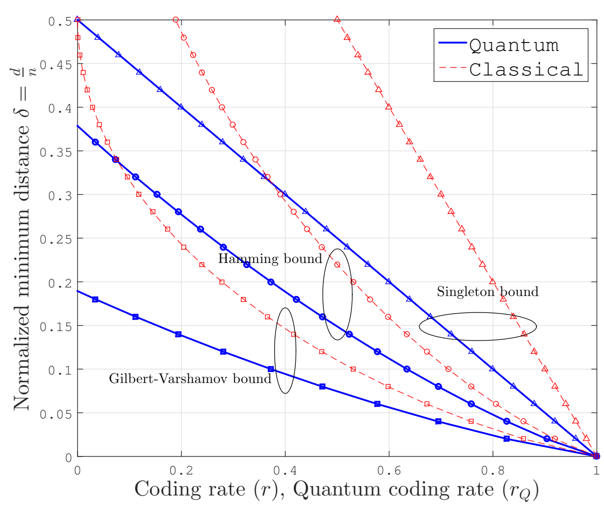

Fig. 9: The evolution from asymptotic classical binary coding bounds to the asymptotic quantum coding bounds.

VI. Quantum Coding Bounds on Asymptotical Limit

Although the classical to binary isomorphism assists us in the development of QSCs from the well-known classical code designs, the issue of determining the actual achieavable minimum distance, given the coding rate and the codeword length still remains unresolved. In the classical domain as we described previously, finding the unique solution to the realistically achievable minimum distance of binary classical codes

TABLE VIII: Comparison of various classical and quantum coding bounds.

Coding Bound	Asymptotic	
	Classical	Quantum
Singleton	$\frac{k}{n} \le 1 - \left(\frac{d}{n}\right)$	$\frac{k}{n} \le 1 - 2\left(\frac{d}{n}\right)$
Hamming	$\frac{k}{n} \le 1 - H\left(\frac{d}{2n}\right)$	$\frac{k}{n} \le 1 - \left(\frac{d}{2n}\right)\log_2 3 - H\left(\frac{d}{2n}\right)$
GV	$\frac{k}{n} \ge 1 - H\left(\frac{d}{n}\right)$	$\frac{k}{n} \ge 1 - \left(\frac{d}{n}\right)\log_2 3 - H\left(\frac{d}{n}\right)$
Coding Bound	Finite-length	
	Classical	Quantum
Singleton	$\frac{k}{n} \le 1 - \left(\frac{d-1}{n}\right)$	$\frac{k}{n} \le 1 - 2\left(\frac{d-1}{n}\right)$
Hamming	$\frac{k}{n} \le 1 - \frac{1}{n}\log_2\left(\sum_{j=0}^{t=\lfloor\frac{d-1}{2}\rfloor}\binom{n}{j}\right)$	$\frac{k}{n} \le 1 - \frac{1}{n}\log_2\left(\sum_{j=0}^{t=\lfloor\frac{d-1}{2}\rfloor}\binom{n}{j}3^j\right)$
GV	$\frac{k}{n} \ge 1 - \frac{1}{n}\log_2\left(\sum_{j=0}^{d-1}\binom{n}{j}\right)$	$\frac{k}{n} \ge 1 - \frac{1}{n}\log_2\left(\sum_{j=0}^{d-1}\binom{n}{j}3^j\right)$

TABLE IX: The coding bounds for classical code constructions, with a minor modification from [65].

Classical Coding Bound	Finite	Asymptotic	Notes
Singleton [75]	$\frac{k}{n} \le 1 - \left(\frac{d-1}{n}\right)$	$\frac{k}{n} \le 1 - \left(\frac{d}{n}\right)$	a loose upper bound
Hamming [76]	$\frac{k}{n} \le 1 - \frac{1}{n}\log_2\left(\sum_{j=0}^{t=\lfloor\frac{d-1}{2}\rfloor}\binom{n}{j}\right)$	$\frac{k}{n} \le 1 - H\left(\frac{d}{2n}\right)$	tight upper bound for very high code rate
MRRW [79]		$\frac{k}{n} \le H\left(\frac{1}{2} - \sqrt{\frac{d}{n}\left(1 - \frac{d}{n}\right)}\right)$	tightest known asymptotic upper bound for medium and low rate codes
Plotkin [80]	$\frac{k}{n} \le \frac{1}{n}\left(1 - \log_2\left(2 - \frac{n}{d}\right)\right)$		tight upper bound for finite-length at $\delta > \frac{1}{2}$
GV [77]	$\frac{k}{n} \ge 1 - \frac{1}{n}\log_2\left(\sum_{j=0}^{d-1}\binom{n}{j}\right)$	$\frac{k}{n} \ge 1 - H\left(\frac{d}{n}\right)$	tightest known lower bound

is still an open problem, even though the upper bound and lower bound of the quantum coding rate versus the achievable minimum distance can be found in the literature [75]–[77], [79], [80]. The bounds for the classical code constructions are listed in Table. IX, while the corresponding asymptotic bounds are also plotted in Fig. 10. In the classical domain, the tightest lower bound was derived by Gilbert [77]. The Hamming bound [76] serves as a tight upper bound for high coding rates, while the McEliece-Rodemich-Rumsey-Welch (MRRW) bound [79] serves as the tightest upper bound for moderate and low coding rates. As seen in Fig. 10, the gap between the tight upper bounds and the lower bound is quite narrow. It was observed in [65] that a simple quadratic expression $r(\delta) = (2\delta - 1)^2$, where δ denotes the normalized minimum distance d/n, satisfies all the known asymptotic bounds.

The well-known bounds for QSC constructions are listed in Table. X and they are also portrayed in Fig. 11. The quantum Singleton bound serves as the loose upper bound, the quantum Hamming bound as a tighter upper bound, and quantum GV bound as the tightest lower bound. However, a wide discrepancy can be observed between the upper bound and the lower bound. For the sake of narrowing this gap, the quantum Rain bound was derived using quantum weight enumerators [81]. To elaborate a little further, the quantum Rain bound states that any quantum code of length n can correct at most $\lfloor\frac{n-1}{6}\rfloor$ errors. The resultant bound is only a

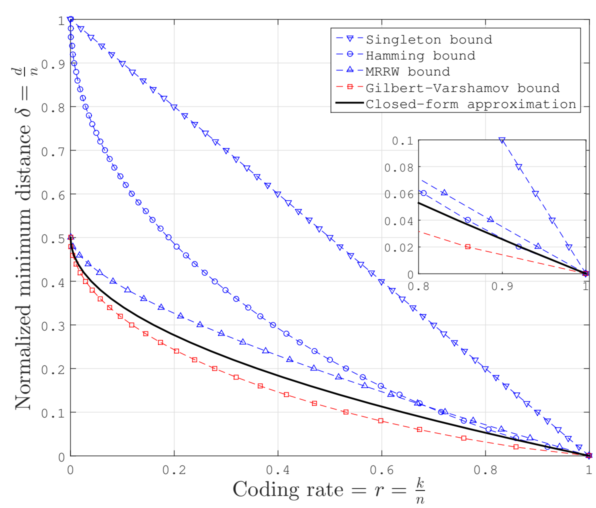

Fig. 10: The trade-off between classical coding rate r and normalized minimum distance δ as described by classical binary coding bounds. A simple quadratic function $r(\delta) = (2\delta - 1)^2$, which satisfies all of the bounds, acts as a closed-form approximation for classical binary error correction codes as suggested in [65].

TABLE X: The well-known quantum coding bounds found in the literature.

Quantum Coding Bound	**Finite-Length**	**Asymptotic**	**Notes**
Singleton [78]	$\frac{k}{n} \leq 1 - 2\left(\frac{d-1}{n}\right)$	$\frac{k}{n} \leq 1 - 2\left(\frac{d}{n}\right)$	very loose upper bound
Hamming [20]	$\frac{k}{n} \leq 1 - \frac{1}{n}\log_2\left(\sum_{j=0}^{t=\lfloor\frac{d-1}{2}\rfloor}\binom{n}{j}3^j\right)$	$\frac{k}{n} \leq 1 - \left(\frac{d}{2n}\right)\log_2 3 - H\left(\frac{d}{2n}\right)$	tight upper bound for moderate and high coding rate
Griesmer-Rain [70], [81]	$\frac{k}{n} \leq 1 - \left(\frac{3d-4}{n}\right)$	$\frac{k}{n} \leq 1 - 3\left(\frac{d}{n}\right)$	tighter upper bound for low coding rates CSS codes
Linear Programming [82]		$\frac{k}{n} \leq H(\tau) + \tau\log_2 3 - 1$ $\tau = \frac{3}{4} - \frac{1}{2}\delta - \frac{1}{2}\sqrt{3\delta(1-\delta)}$	strengthen the upper bound
GV [20]	$\frac{k}{n} \geq 1 - \frac{1}{n}\log_2\left(\sum_{j=0}^{d-1}\binom{n}{j}3^j\right)$	$\frac{k}{n} \geq 1 - \left(\frac{d}{n}\right)\log_2 3 - H\left(\frac{d}{n}\right)$	tight lower bound for general stabilizer codes
GV for CSS [66]		$\frac{k}{n} \geq 1 - 2H\left(\frac{d}{n}\right)$	tight lower bound for CSS codes
	$\frac{k}{n} \geq 1 - \frac{2}{n}\log_2\left(\sum_{j=0}^{d-1}\binom{n}{j}\right)$		lower bound for dual-containing CSS codes

function of codeword length n. Hence, under the asymptotic limit, the quantum Rain bound is a straigthline at $\delta = 1/3$, which does not exhibit any further trade-off between the quantum coding rate and the minimum distance. In order to enhance the accuracy of the quantum Rain bound, Sarvepalli and Klappenecker derived a quantum version of Griesmer bound [70]. By utilizing the quantum Griesmer bound and also the quantum Rain bound, a stronger bound was created for CSS type constructions. In this treatise we will refer to this particular bound as the quantum Griesmer-Rain bound. For the sake of tightening the upper bound, Ashikhmin and Litsyn generalized the classical linear programming approach to the quantum domain using the MacWilliams identities [82]. The resultant quantum linear programming bound was proven to be tighter than the quantum Hamming bound in the low coding rate domain. As the quantum coding rate approaches zero, the achievable mormalized minimum distance returned by the quantum Griesmer-Rain bound becomes $\delta = 0.3333$ and that of quantum linear programming bound becomes $\delta = 0.3152$.

Recall from Section III that the QSCs may exhibit either a CSS or non-CSS structure. For CSS codes, the minimum distance is upper-bounded by the quantum Hamming bound for moderate to high quantum coding rates and by the quantum Griesmer-Rain bound for low coding rates region, while it is also lower-bounded by the quantum GV bound for CSS codes. On the other hand, for non-CSS QSCs, the minimum distance is upper-bounded by the quantum Hamming bound for moderate to high coding rates and by the quantum linear-programming bound for low coding rates. It is also lower-bounded by the quantum GV bound for general quantum stabilizer codes. Even though substantial efforts have been invested tightening the gap between the upper and lower bounds, a significant amount of discrepancy persists. Hence, creating a simple approximation may be beneficial for giving us further insights into the realistic construction of QSCs.

Analogous to the classical closed-form approximation of [65], we also found that there exists a simple closed-form quadratic approximation, which satisfies all the well-known quantum coding bounds. Explicitly for quantum stabilizer codes, the following quadratic function was found to satisfy all the quantum coding bounds:

$$r_Q(\delta) = \frac{32}{9}\delta^2 - \frac{16}{3}\delta + 1 \text{ for } 0 \leq \delta \leq 0.2197. \quad (75)$$

We will further elaborate on the selection of this function in Section VIII. It is important to note that the closed-form approximation is subject to the asymptotical bound for either CSS type or non-CSS type quantum code constructions. The closed-form approximation in Eq. (75) offers the benefit of simplicity and it has the inverse function as given by

$$\delta(r_Q) = \frac{3\left(\sqrt{2} - \sqrt{r_Q + 1}\right)}{4\sqrt{2}} \text{ for } 0 \leq r_Q \leq 1. \quad (76)$$

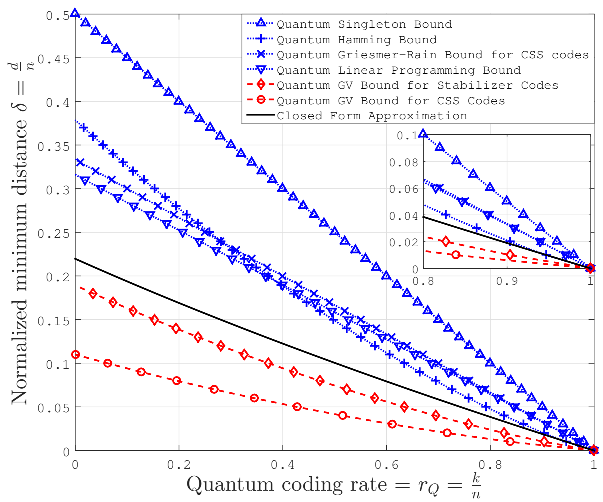

Fig. 11: The trade-off between quantum coding rate r_Q and normalized minimum distance δ is characterized using quantum coding bounds. A simple quadratic closed-form $r_Q(\delta) = \frac{32}{9}\delta^2 - \frac{16}{3}\delta + 1$ satisfies all of the well-known quantum coding bounds, which is portrayed by black solid lines. The blue dashed lines portrays the upper bounds, while the red dashed lines denotes the lower bounds.

This closed-form approximation suggests that it is possible to create a code construction whose minimum distance grows linearly with the codeword length at the asymptotical limit since for a given quantum coding rate r_Q, it will correspond to a unique constant value of δ.

VII. Quantum Coding Bounds on Finite-Length Codes

The asymptotic limits are only relevant for $n \to \infty$. For practical applications, we require code constructions with shorter codeword length, which necessitates a different formulation for the quantum coding bounds. Finding a closed-form approximation will be beneficial for determining the realistically attainable minimum distance for the given code parameters. The well-known quantum coding bounds are listed in Table X and also portrayed in Fig. 11. It is clearly seen that a simple quadratic approximation can satisfy all the well-known bounds. For the finite-length quantum codes, we propose the closed-form approximation of

$$r_Q(n,\delta) = a\delta^2 + b\delta + c. \tag{77}$$

To arrive at the closed-form approximation in Eq. (77), we have to determine three definitive points corresponding to realistic quantum code constructions. As an example in this treatise, we use three QSC constructions from the literature as listed below:

- For uncoded logical qubits and unity rate codewords, we have
$$r_Q(n,\delta) = r(n, \frac{1}{n}) = 1. \tag{78}$$
- For a high coding rate, we will use the construction given in [19]. For $n = 2^j$, there is a quantum stabilizer code construction $[n,k,d] = [n, n-j-2, 3]$, which can be used to correct $t = 1$ error. This code construction reaches the quantum Hamming bound. For arbitrary n, it can be written as
$$r_Q(n,\delta) = r(n, \frac{3}{n}) = 1 - \frac{1}{n}\log_2(n) - \frac{2}{n}. \tag{79}$$
- For a very low coding rate, we are using the quantum stabilizer code constructions derived from quadratic residues [83], [84]. By using simple linear regression, we arrive at
$$r_Q(n,\delta) = r(n, \frac{2}{n} + \frac{1}{4}) = \frac{1}{n}. \tag{80}$$

Using the three definitive points from the constructions given in Eq. (78), (79) and (80), we arrive at a system of three linear equations, which have a unique value of a, b and c for an arbitrary value of n. More explicitly, we have

$$r_1 = a\delta_1^2 + b\delta_1 + c, \tag{81}$$
$$r_2 = a\delta_2^2 + b\delta_2 + c, \tag{82}$$
$$r_3 = a\delta_3^2 + b\delta_3 + c. \tag{83}$$

The analytical solution of Eq. (81), (82), and (83) is based on the following unique parameter values:

$$a = \frac{(r_3 - r_2)\,\delta_1 + (r_1 - r_3)\,\delta_2 + (r_2 - r_1)\,\delta_3}{(\delta_2 - \delta_1)\,(\delta_3 - \delta_2)\,(\delta_1 - \delta_3)}, \tag{84}$$
$$b = \frac{(r_2 - r_3)\,\delta_1^2 + (r_3 - r_1)\,\delta_2^2 + (r_1 - r_2)\,\delta_3^2}{(\delta_2 - \delta_1)\,(\delta_3 - \delta_2)\,(\delta_1 - \delta_3)}, \tag{85}$$
$$c = \frac{(r_3\delta_2 - r_2\delta_3)\,\delta_1^2 + (r_1\delta_3 - r_3\delta_1)\,\delta_2^2 + (r_2\delta_1 - r_1\delta_2)\,\delta_3^2}{(\delta_2 - \delta_1)\,(\delta_3 - \delta_2)\,(\delta_1 - \delta_3)}. \tag{86}$$

Despite the cluttered appearance of the analytical solution, it contains a simple closed-form approximation, because the value of r_1, r_2, r_3, δ_1, δ_2 and δ_3 may be easily calculated using Eq. (78), (79) and (80). Furthermore, the closed-form approximation derived for finite-length codewords has an inverse function of

$$\delta(n, r_Q) = \frac{-b - \sqrt{b^2 - 4a(c - r_Q)}}{2a}. \tag{87}$$

The accuracy of the proposed method is now tested for QSCs having codeword length of $n = \{31, 32, 63, 64, 127, 128\}$ as shown in Fig. 12. The list of practical QSC constructions which are used in these plots can be seen in Table. XI[4]. The closed-form approximation lies entirely between the upper and the lower quantum coding bounds. The practical QSCs are also plotted in the same figure to show the relative position with respect to the quantum coding bounds. The QSCs based on [22], [26] lays perfectly on approximation curves, but it has been observed in [85] that as the codeword length increases and the quantum coding rate is reduced, the exact value of the minimum distance becomes unclear. As depicted in Fig. 12b and 12c, we can hardly find definitive points associated with actual codes to plot in the low quantum coding-rate region constructed from quantum $GF(4)$. Meanwhile, the QBCH code constructions lie quite close to the GV lower bound for dual-containing CSS codes. As predicted, since the constructions of QBCH codes rely on dual-containing CSS type constructions, which employ two separate PCMs for their stabilizer operators, we expect a lower coding rate compared to their non-CSS relatives.

The proposed closed-form approximation offers substantial benefits for the development of QSCs. We can readily find a fairly precise approximation of the realistically achievable minimum distance for given code parameters. For instance, for half-rate quantum stabilizer codes of length 128, the minimum distance is bounded by $11 < d < 22$. By using our formulation, we obtain $d(n = 128, r_Q = 1/2) = 16$ from our finite-length approximation. Likewise, for half-rate quantum stabilizer codes of length 1024, the minimum distance is bounded by $78 < d < 157$. Using our method, we can obtain $d(n = 1024, r_Q = 1/2) = 103$ from our asymptotic bound approximation. One of the logical questions that may arise concerns the existence of the corresponding codes. For example, does a half-rate QSCs relying on $n = 128$ physical qubits and a minimum distance of $d = 16$ exist? The answer to this question is not definitive. Let us refer to the code

[4] A comprehensive list of practical quantum stabilizer codes can be found online at [85]. In this treatise, we only consider quantum stabilizer codes with definitive minimum distance in the list.

TABLE XI: The list of QSC constructions that are used to plot practical code in Fig. 12.

$\mathcal{C}[n,k,d]$ for $n=31$ and $n=32$	
QBCH [23]	[31,1,7], [31,11,5], [31,21,3]
QRM [26]	[32,10,6], [32,25,3]
QGF(4) [22]	[31,1,11], [31,2,10], [31,21,4], [31,26,2], [32,1,11], [32,16,6], [32,22,4], [32,25,3], [32,30,2]
$\mathcal{C}[n,k,d]$ for $n=63$ and $n=64$	
QBCH [23]	[63,27,7], [63,39,5], [63,45,4], [63,51,3], [63,57,2]
QRM [26]	[64,35,6], [64,56,3]
QGF(4) [22]	[63,51,4], [63,55,3], [63,60,2], [64,44,6], [64,48,5], [64,52,4], [64,56,3], [64,62,2]
$\mathcal{C}[n,k,d]$ for $n=127$ and $n=128$	
QBCH [23]	[127,1,19], [127,15,16], [127,29,15], [127,43,13], [127,57,11], [127,71,9], [127,85,7], [127,99,5], [127,113,3]
QRM [26]	[128,35,12], [128,91,6], [128,119,3]
QGF(4) [22]	[127,114,4], [127,118,3], [127,124,2], [128,105,6], [128,110,5], [128,114,4], [128,119,3], [128,126,2]

table given in [85], which is mainly based on the QSC constructions of [22]. Due to space limitations, we are unable to capture the entire table and the associated PCM formulation. However, it is shown in [85] that a half-rate QSC relying on $n = 128$ physical qubits indeed exists, although the minimum distance is only loosely specified by the bounds of $11 < d < 20$. The bound is similar to the quantum GV bound and to the quantum Hamming bound of the minimum distance given by $11 < d < 22$. By contrast, upon using our approximation, we have a minimum distance of $d = 16$, which is again only an approximation and it does not imply the existence of a quantum code having a similar minimum distance. Nonetheless, we believe that our approximation is beneficial for approximating the attainable QBER performance of QSCs based on hard-decision syndrome decoding for short to moderate codeword length as follows (without considering degeneracy):

$$\text{QBER}(n,d,p) = 1 - \sum_{i=0}^{t=\lfloor\frac{d-1}{2}\rfloor} \binom{n}{i} p^i (1-p)^{n-i}, \tag{88}$$

where the realistically achievable value of d is obtained from our approximation. In our view, the combination of our closed-form approximation and the QBER of Eq. (88) constitutes a useful benchmarker for the future development of QSCs, since it quantifies the realistically achievable QBER performance based on hard-decision syndrome-based decoding.

The evolution of our closed-form approximation as the codeword length increases for $n = \{31, 32, 63, 64, 127, 128\}$ can be seen in Fig. 13. By using our example, it can be clearly observed that as the codeword length increases, the derived approximation for finite-length codes slowly approaches the closed-form approximation of the asymptotic bound. However, inaccuracies emerge as the codeword length increases. This phenomenon is due to the fact that we do not have a definitive QSC constructions to rely on in the low coding rate region. In our approximation example, we are using the QSCs from quadratic residues construction for low coding rate region and the number of QSC constructions are very limited only for a handful codeword lengths. Meanwhile in the classsical domain, in the low coding rate region, we have the simple repetition codes, with construction $\mathcal{C}(n,1)$ having a normalized minimum distance of $\delta(n,r) = \delta(n,\frac{1}{n}) = 1$.

Albeit the finite and infinite-length-based approximation curves start to deviate for a very long codeword $n \gg 100$, the minimum distance still grows as the codeword length increases as portrayed in Fig. 14. Both the finite-length approximation and asymptotic approximation follow the same trend. For $n \gg 100$, we can simply utilize the asymptotic formulation given in Eq. (75) for calculating the quantum coding rate for a certain desired minimum distance, or the inverse of the asymptotic formulation in Eq. (76) to determine the realistically achievable minimum distance given the quantum coding rate. We can conclude from this figure that it is indeed possible to have a QSC construction with a growing minimum distance, as the codeword length increases.

VIII. The Bounds on Entanglement-Assisted Quantum Stabilizer Codes

One of the distinctive characteristics of quantum systems, which does not bear any resemblance with the classical domain is the ability of creating entanglement. This unique property can be exploited for increasing the achievable minimum distance of quantum codes, hence increasing the error correction capability of QSCs. The EA-QSC constructions are denoted by $\mathcal{C}(n,k;c)$, where c denotes the number of preshared entangled qubits. It is important to note that even though the EA-QSCs expand the Pauli group operators from $\mathcal{G}^n$ into $\mathcal{G}^{n+c}$, we only consider the error operators in $\mathcal{G}^n$. This is because the paradigm of EA-QSCs assumes that the preshared entangled qubits are not subjected to transmission error. Hence, for EA-QSCs, the quantum Hamming bound of Eq. (64) can be modified to

$$2^k \leq \frac{2^{n+c}}{\sum\limits_{j=0}^{t=\lfloor\frac{d_{ea}-1}{2}\rfloor} \binom{n}{j} 3^j}, \tag{89}$$

where the notation d_{ea} denotes the minimum distance of EA-QSCs. Equation (89), can be rewritten to show explicitly the trade-off between quantum coding rate r_Q and minimum distance d_{ea} on EA-QSCs as follows:

$$\frac{k}{n} \leq 1 - \frac{1}{n}\log_2\left(\sum_{j=0}^{t=\lfloor\frac{d_{ea}-1}{2}\rfloor} \binom{n}{j} 3^j\right) + \left(\frac{c}{n}\right). \tag{90}$$

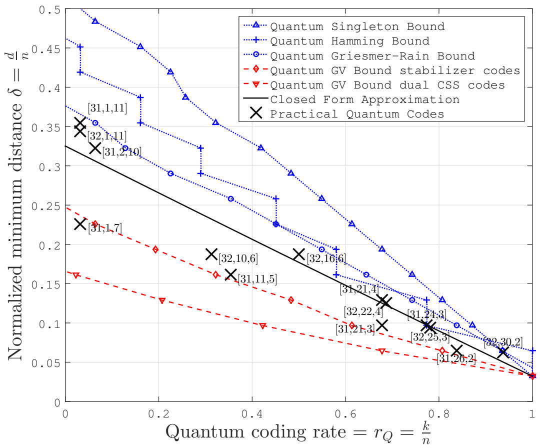

(a) ($n = 31$) and ($n = 32$)

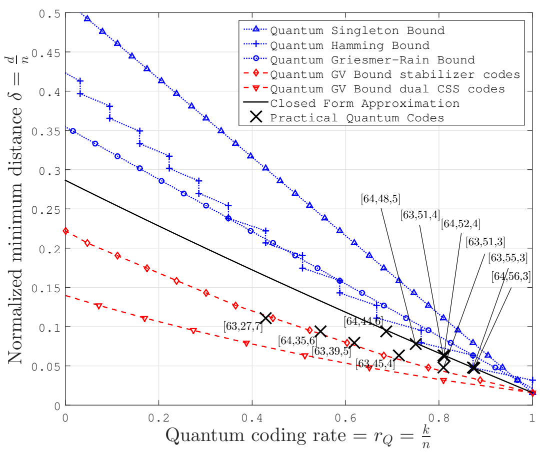

(b) ($n = 63$) and ($n = 64$)

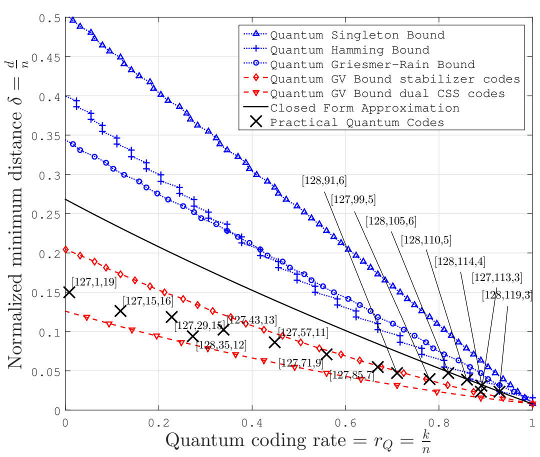

(c) ($n = 127$) and ($n = 128$)

Fig. 12: Quantum coding rate r_Q versus normalized minimum distance δ for finite-length QSCs. The points for portraying the practical QSCs are taken from QBCH codes [23], QRM codes [26] and quantum codes from $GF(4)$ formulation [22].

When n tends to ∞, we yield

$$\frac{k}{n} \leq 1 - \left(\frac{d_{ea}}{2n}\right) \log_2 3 - H\left(\frac{d_{ea}}{2n}\right) + \left(\frac{c}{n}\right). \qquad (91)$$

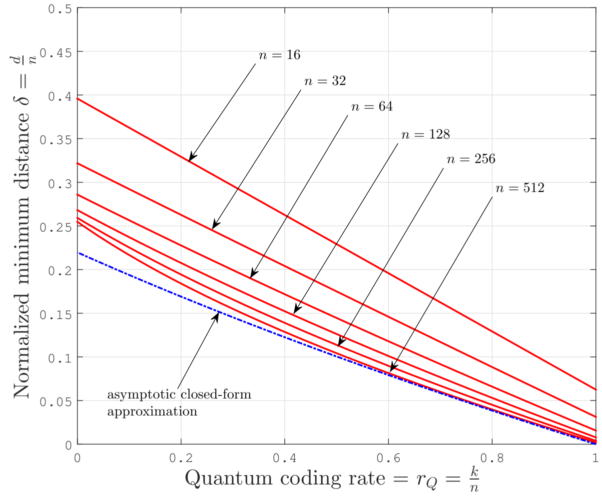

Fig. 13: The evolution of our closed-form approximation for finite-length codewords for various values of codeword length n.

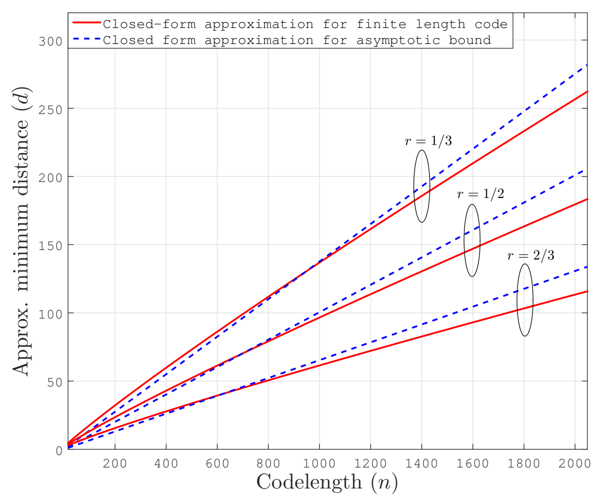

Fig. 14: The growth of achievable minimum distance for short block QSCs as the codeword length increasing.

As encapsulated in Eq. (91), an additional conflicting parameter is involved in determining the quantum coding bounds, namely the entanglement consumption rate. The entanglement consumption rate E is the ratio between the number of preshared maximally entangled qubits c to the number of physical qubits n as encapsulated below:

$$E = \frac{c}{n}. \qquad (92)$$

A maximally entangled[5] QSCs requires $c = n - k$ preshared qubit pairs. Hence, for a maximally entangled QSCs, the

[5]For a maximally-entangled QSCs, all of the auxiliary qubits required to generate the encoded state are already preshared using maximally entangled pair qubits. Hence, the maximal number of entangled pair qubits that can be shared beforehand is equal to the total number of auxiliary qubits, which is equal to $(n - k)$

quantum Hamming bound of Eq. (91) can be reformulated as follows by substituting $c = n - k$ into Eq. (91), yielding:

$$\frac{k}{n} \leq 1 - \frac{1}{2}\left(\left(\frac{d_{ea}}{2n}\right)\log_2 3 - H\left(\frac{d_{ea}}{2n}\right)\right). \tag{93}$$

Let us how consider the more general cases, where we may have a range of different entanglement ratios $0 \leq \theta \leq 1$. The entanglement ratio is defined as the ratio of preshared qubits c to the maximally-entangled preshared qubits $(n-k)$, yielding:

$$\theta = \frac{c}{n-k}. \tag{94}$$

The quantum Hamming bound for EA-QSCs with arbitrary entanglement ratios of θ is given by

$$\frac{k}{n} \leq 1 - \frac{1}{1+\theta}\left(\left(\frac{d_{ea}}{2n}\right)\log_2 3 - H\left(\frac{d_{ea}}{2n}\right)\right). \tag{95}$$

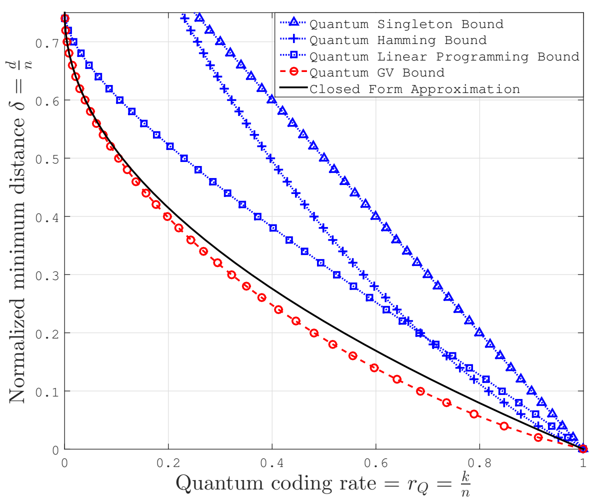

Fig. 15: The asymptotic quantum coding bounds on EA-QSCs for maximally-entangled constructions. A simple quadratic function $r(\delta) = \frac{16}{9}\delta^2 - \frac{8}{3}\delta + 1$ satisfies all of the quantum coding bounds.

The rest of the quantum coding bounds can readily be derived using the same analogy. The resultant entanglement-assisted quantum coding bounds are portrayed in Fig. 15 and 16. By substituting the entanglement ratio of $\theta = 0$, we arrive again at the quantum coding bounds derived for unassisted QSCs. By contrast, upon substituting into Eq. (95) the entanglement ratio $\theta = 1$, we have the quantum coding bounds for maximally-entangled QSCs. Figure 15 portrays the bounds on maximally-entangled QSCs. It is observed in Fig. 15 that at the point $(\delta = 0.75)$, the quantum GV bound (lower bound) intersects the quantum linear programming bound (upper bound). Indeed, it is confirmed by the quantum Plotkin bound for the maximally-entangled QSC constructions shown in Table XIII that for asymptotical maximally-entangled QSCs the highest normalized minimum distance that can be achieved is $\delta = 0.75$. Hence, based on this observation, we propose a simple quadratic function as the closed-form approximation of entanglement-assisted quantum stabilizer codes that

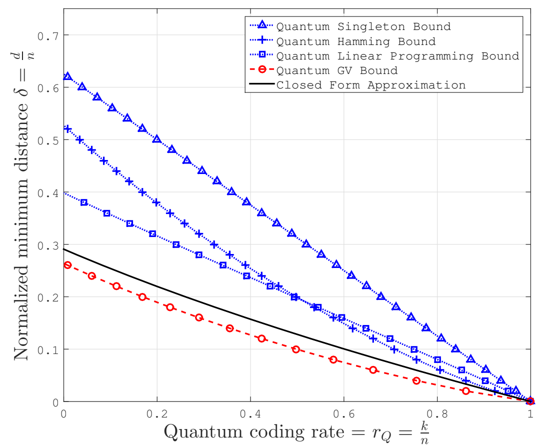

(a) $\theta = 0.25$

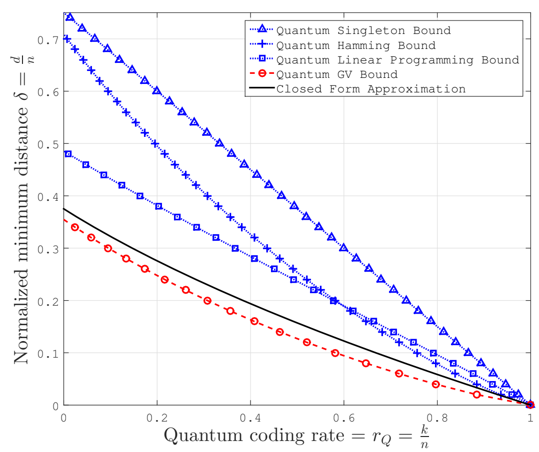

(b) $\theta = 0.5$

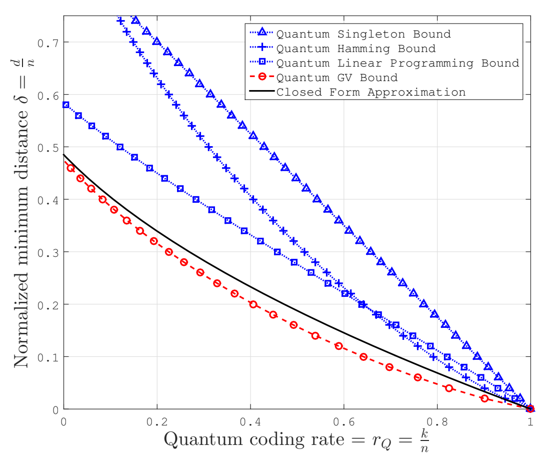

(c) $\theta = 0.75$

Fig. 16: The asymptotic quantum coding bounds on EA-QSCs for different entanglement ratios.

will satisfy all of the well-known bounds. A quadratic function associated with a symmetry line at $(\delta = 0.75)$ and crossing

TABLE XII: The entanglement-assisted quantum coding bounds found in the literature.

Quantum Coding Bound	Finite-Length	Asymptotic	Notes
Singleton [49]	$\frac{k}{n} \leq 1-2\left(\frac{d_{ea}-1}{n}\right)+\left(\frac{c}{n}\right)$	$\frac{k}{n} \leq 1-2\left(\frac{d_{ea}}{n}\right)+\left(\frac{c}{n}\right)$	very loose upper bound
Hamming [48]	$\frac{k}{n} \leq 1-\frac{1}{n}\log_2\left(\sum_{j=0}^{t=\lfloor\frac{d_{ea}-1}{2}\rfloor}\binom{n}{j}3^j\right)+\left(\frac{c}{n}\right)$	$\frac{k}{n} \leq 1-\left(\frac{d_{ea}}{2n}\right)\log_2 3-H\left(\frac{d_{ea}}{2n}\right)+\left(\frac{c}{n}\right)$	tight upper bound
Linear Programming [86]		$\frac{k}{n} \leq H(\tau)+\tau\log_2 3-1+\left(\frac{c}{n}\right)$ $\tau=\frac{3}{4}-\frac{1}{2}\delta-\frac{1}{2}\sqrt{3\delta(1-\delta)}$	strengthen the upper bound
Plotkin [87], [88]	$\frac{d_{ea}}{n} \leq \frac{3(4^k)}{8(4^k-1)}\left(1+\left(\frac{k}{n}\right)+\left(\frac{c}{n}\right)\right)$	$\frac{d_{ea}}{n} \leq \frac{3}{8}\left(1+\left(\frac{k}{n}\right)+\left(\frac{c}{n}\right)\right)$	upper bound for minimum distance
GV [88]	$\frac{k}{n} \geq 1-\frac{1}{n}\log_2\left(\sum_{j=0}^{d_{ea}-1}\binom{n}{j}3^j\right)+\left(\frac{c}{n}\right)$	$\frac{k}{n} \geq 1-\left(\frac{d_{ea}}{n}\right)\log_2 3-H\left(\frac{d_{ea}}{n}\right)+\left(\frac{c}{n}\right)$	tight lower bound

TABLE XIII: The asymptotic quantum coding bounds for EA-QSCs given the arbitrary entanglement ratios of θ.

Quantum Coding Bound	Entanglement Ratio $=\theta$	Maximally Entangled $(\theta=1)$
Singleton [49]	$\frac{k}{n} \leq 1-\left(\frac{2}{1+\theta}\right)\left(\frac{d_{ea}}{n}\right)$	$\frac{k}{n} \leq 1-\left(\frac{d_{ea}}{n}\right)$
Hamming [48]	$\frac{k}{n} \leq 1-\frac{1}{1+\theta}\left(\left(\frac{d_{ea}}{2n}\right)\log_2 3-H\left(\frac{d_{ea}}{2n}\right)\right)$	$\frac{k}{n} \leq 1-\frac{1}{2}\left(\left(\frac{d_{ea}}{2n}\right)\log_2 3-H\left(\frac{d_{ea}}{2n}\right)\right)$
Linear Programming [86]	$\frac{k}{n} \leq \frac{1}{1+\theta}\left(H(\tau)+\tau\log_2 3-1+\theta\right)$	$\frac{k}{n} \leq \frac{1}{2}\left(H(\tau)+\tau\log_2 3\right)$
Plotkin [87], [88]	$\frac{d_{ea}}{n} \leq \frac{3}{8}\left(1+\theta+\frac{k}{n}(1-\theta)\right)$	$\frac{d_{ea}}{n} \leq \frac{3}{4}$
GV [88]	$\frac{k}{n} \geq 1-\frac{1}{1+\theta}\left(\left(\frac{d_{ea}}{n}\right)\log_2 3-H\left(\frac{d_{ea}}{n}\right)\right)$	$\frac{k}{n} \geq 1-\frac{1}{2}\left(\left(\frac{d_{ea}}{n}\right)\log_2 3-H\left(\frac{d_{ea}}{n}\right)\right)$

the point of $(\delta, r)=(0,1)$ is given by

$$r_Q(\delta)=\frac{16}{9}\delta^2-\frac{8}{3}\delta+1 \text{ for } 0 \leq \delta \leq 0.75. \tag{96}$$

The simple quadratic approximaton given in Eq. (96), can also be inverted, yielding

$$\delta(r_Q)=\frac{3}{4}(1-\sqrt{r_Q}) \text{ for } 0 \leq r_Q \leq 1. \tag{97}$$

From the simple quadratic function in Eq. (96), we can also derive a simple closed-form approximation for a given arbitrary entanglement ratio of $0 \leq \theta \leq 1$, as shown below:

$$r_Q(\delta)=\frac{1}{1+\theta}\left(\frac{32}{9}\delta^2-\frac{16}{3}\delta+1+\theta\right), \tag{98}$$

for $0 \leq \delta \leq \frac{3}{4}\left(1-\sqrt{\frac{1-\theta}{2}}\right)$ and $0 \leq \theta \leq 1$. The expression given in Eq. (98) may be inverted to arrive at the following equation:

$$\delta(r_Q)=\frac{3(\sqrt{2}-\sqrt{r_Q(1+\theta)+(1-\theta)}}{4\sqrt{2}}, \tag{99}$$

for $0 \leq r_Q \leq 1$ and $0 \leq \theta \leq 1$. The simple closed-form approximation given in Eq. (98) and (99) satisfies all entanglement-assisted quantum coding bounds for arbitrary entanglement ratios, as confirmed by Fig. 16. We should point out at this stage that as we substitute the value of $\theta=0$ into Eq. (98) and (99), we comeback with the closed-form approximation presented in the Eq. (75) and (76) for unassisted asymptotic quantum coding bounds. Hence, we completed our closed-form approximations conceived for all of different constructions of quantum stabilizer codes.

IX. Conclusions

We have conducted a survey of quantum coding bounds, which describe the trade-off between the quantum coding rate and the error correction capability for a wide range of QSC constructions. Furthermore, we provided insights on their relationships with their classical counterparts. For the family of unassisted QSCs, we have provided both lower and upper bounds for both CSS and non-CSS code constructions. For the EA-QSCs, we have presented the quantum coding bounds for maximally-entangled constructions and also for arbitrary entanglement ratios.

We also have proposed a closed-form approximation as a beneficial tool for analyzing the performance of QSCs. The resultant closed-form approximation may be indeed used as a simple benchmark for developing QSCs, because the resultant minimum distance δ and quantum coding rate r_Q values from our approximations are unambiguous. For instance, for a half-rate quantum stabilizer code having a given codeword length of $n=128$, the minimum distance is bounded by $11<d<22$. By using our approximation, we arrive at $d(n=128, r_Q=1/2)=16$ from our finite-length approximation. Likewise, for a half-rate quantum stabilizer code having the codeword length of 1024, the minimum distance is bounded by $78<d<157$. By using our proposal, we have an approximate minimum distance of $d(n=1024, r_Q=1/2)=103$ from our asymptotic bound approximation. Ultimately, the proposed method can be utilized as an efficient tool for the characterization of quantum stabilizer codes.

References

[1] L. Hanzo, H. Haas, S. Imre, D. O'Brien, M. Rupp, and L. Gyongyosi, "Wireless myths, realities, and futures: from 3G/4G to optical and quantum wireless," *Proceedings of the IEEE (Special Centennial Issue)*, vol. 100, pp. 1853–1888, 2012.

[2] M. M. Waldrop, "The chips are down for Moores law," *Nature News*, vol. 530, pp. 144–147, 2016.

[3] P. W. Shor, "Algorithms for quantum computation: Discrete logarithms and factoring," in *Proceedings of 35th Annual Symposium on Foundations of Computer Science, 1994*, pp. 124–134, 1994.

[4] P. W. Shor, "Polynomial-time algorithms for prime factorization and discrete logarithms on a quantum computer," *SIAM Review*, vol. 41, no. 2, pp. 303–332, 1999.

[5] L. K. Grover, "A fast quantum mechanical algorithm for database search," in *Proceedings of 28th Annual ACM Symposium on Theory of Computing, 1996*, pp. 212–219, 1996.

[6] M. Boyer, G. Brassard, P. Høyer, and A. Tapp, "Tight bounds on quantum searching," *arXiv preprint quant-ph/9605034*, 1996.

[7] C. Durr and P. Hoyer, "A quantum algorithm for finding the minimum," *arXiv preprint quant-ph/9607014*, 1996.

[8] L. K. Grover, "Quantum mechanics helps in searching for a needle in a haystack," *Physical Review Letters*, vol. 79, no. 2, 1997.

[9] C. Zalka, "Grovers quantum searching algorithm is optimal," *Physical Review A*, vol. 60, no. 4, 1999.

[10] G. Brassard, F. Dupuis, S. Gambs, and A. Tapp, "An optimal quantum algorithm to approximate the mean and its application for approximating the median of a set of points over an arbitrary distance," *arXiv preprint arXiv:1106.4267*, 2011.

[11] P. Botsinis, S. X. Ng, and L. Hanzo, "Quantum search algorithms, quantum wireless, and a low-complexity maximum likelihood iterative quantum multi-user detector design," *IEEE Access*, vol. 1, pp. 94–122, 2013.

[12] P. Botsinis, D. Alanis, S. X. Ng, and L. Hanzo, "Low-complexity soft-output quantum-assisted multiuser detection for direct-sequence spreading and slow subcarrier-hopping aided SDMA-OFDM systems," *IEEE Access*, vol. 2, pp. 451–472, 2014.

[13] D. Alanis, P. Botsinis, S. X. Ng, and L. Hanzo, "Quantum-assisted routing optimization for self-organizing networks," *IEEE Access*, vol. 2, pp. 614–632, 2014.

[14] D. Alanis, P. Botsinis, Z. Babar, S. X. Ng, and L. Hanzo, "Non-dominated quantum iterative routing optimization for wireless multihop networks," *IEEE Access*, vol. 3, pp. 1704–1728, 2015.

[15] D. P. DiVincenzo, "The physical implementation of quantum computation," *Fortschritte der Physik*, vol. 48, no. 9-11, pp. 771–783, 2000.

[16] P. W. Shor, "Scheme for reducing decoherence in quantum computer memory," *Physical Review A*, vol. 52, no. 4, 1995.

[17] A. M. Steane, "Error correcting codes in quantum theory," *Physical Review Letters*, vol. 77, no. 5, 1996.

[18] R. Laflamme, C. Miquel, J. P. Paz, and W. H. Zurek, "Perfect quantum error correcting code," *Physical Review Letters*, vol. 77, no. 1, 1996.

[19] D. Gottesman, "Class of quantum error-correcting codes saturating the quantum Hamming bound," *Physical Review A*, vol. 54, no. 3, 1996.

[20] A. Ekert and C. Macchiavello, "Quantum error correction for communication," *Physical Review Letters*, vol. 77, no. 12, 1996.

[21] D. Gottesman, *Stabilizer codes and quantum error correction*. PhD thesis, California Institute of Technology, 1997.

[22] A. R. Calderbank, E. M. Rains, P. W. Shor, and N. J. Sloane, "Quantum error correction via codes over GF(4)," *IEEE Transactions on Information Theory*, vol. 44, no. 4, pp. 1369–1387, 1998.

[23] M. Grassl and T. Beth, "Quantum BCH codes," in *Proceedings of International Symposium Theoretical Electrical Engineering, 1999*, 1999.

[24] M. Grassl, T. Beth, and T. Pellizzari, "Codes for the quantum erasure channel," *Physical Review A*, vol. 56, no. 1, 1997.

[25] M. Grassl, W. Geiselmann, and T. Beth, "Quantum Reed-Solomon codes," in *Applied Algebra, Algebraic Algorithms and Error-Correcting Codes*, pp. 231–244, Springer, 1999.

[26] A. M. Steane, "Quantum Reed-Muller codes," *IEEE Transactions on Information Theory*, vol. 45, no. 5, pp. 1701–1703, 1999.

[27] H. F. Chau, "Quantum convolutional error-correcting codes," *Physical Review A*, vol. 58, no. 2, 1998.

[28] H. Ollivier and J.-P. Tillich, "Description of a quantum convolutional code," *Physical Review Letters*, vol. 91, no. 17, 2003.

[29] D. J. MacKay, G. Mitchison, and P. L. McFadden, "Sparse-graph codes for quantum error correction," *IEEE Transactions on Information Theory*, vol. 50, no. 10, pp. 2315–2330, 2004.

[30] D. Poulin, J.-P. Tillich, and H. Ollivier, "Quantum serial turbo codes," *IEEE Transactions on Information Theory*, vol. 55, no. 6, pp. 2776–2798, 2009.

[31] J. M. Renes, F. Dupuis, and R. Renner, "Efficient polar coding of quantum information," *Physical Review Letters*, vol. 109, no. 5, 2012.

[32] A. Y. Kitaev, "Quantum computations: Algorithms and error correction," *Russian Mathematical Surveys*, vol. 52, no. 6, pp. 1191–1249, 1997.

[33] A. Y. Kitaev, "Fault-tolerant quantum computation by anyons," *Annals of Physics*, vol. 303, no. 1, pp. 2–30, 2003.

[34] M. H. Freedman, D. A. Meyer, and F. Luo, "Z2-systolic freedom and quantum codes," *Mathematics of quantum computation*, pp. 287–320, 2002.

[35] S. B. Bravyi and A. Y. Kitaev, "Quantum codes on a lattice with boundary," *arXiv preprint quant-ph/9811052*, 1998.

[36] C. Horsman, A. G. Fowler, S. Devitt, and R. Van Meter, "Surface code quantum computing by lattice surgery," *New Journal of Physics*, vol. 14, no. 12, 2012.

[37] H. Bombin and M. A. Martin-Delgado, "Topological quantum distillation," *Physical Review Letters*, vol. 97, no. 18, 2006.

[38] J. Haah, "Local stabilizer codes in three dimensions without string logical operators," *Physical Review A*, vol. 83, no. 4, 2011.

[39] G. Zémor, "On Cayley graphs, surface codes, and the limits of homological coding for quantum error correction," in *Proceedings of International Conference on Coding and Cryptology, 2009*, pp. 259–273, 2009.

[40] A. Couvreur, N. Delfosse, and G. Zemor, "A construction of quantum LDPC codes from Cayley graphs," *IEEE Transactions on Information Theory*, vol. 59, no. 9, pp. 6087–6098, 2013.

[41] N. Delfosse, "Tradeoffs for reliable quantum information storage in surface codes and color codes," in *Proceedings of IEEE International Symposium on Information Theory (ISIT), 2013*, pp. 917–921, 2013.

[42] J.-P. Tillich and G. Zémor, "Quantum LDPC codes with positive rate and minimum distance proportional to the square root of the blocklength," in *Proceedings of IEEE International Symposium on Information Theory (ISIT), 2009*, pp. 799–803, 2009.

[43] A. A. Kovalev and L. P. Pryadko, "Improved quantum hypergraph-product LDPC codes," in *Proceedings of IEEE International Symposium on Information Theory (ISIT), 2012*, pp. 348–352, 2012.

[44] J.-P. Tillich and G. Zémor, "Quantum LDPC codes with positive rate and minimum distance proportional to the square root of the blocklength," *IEEE Transactions on Information Theory*, vol. 60, no. 2, pp. 1193–1202, 2014.

[45] S. Bravyi and M. B. Hastings, "Homological product codes," in *Proceedings of the 46th Annual ACM Symposium on Theory of Computing, 2014*, pp. 273–282, 2014.

[46] D. A. Lidar and T. A. Brun, *Quantum error correction*. Cambridge University Press, 2013.

[47] A. R. Calderbank, E. M. Rains, P. W. Shor, and N. J. Sloane, "Quantum error correction and orthogonal geometry," *Physical Review Letters*, vol. 78, no. 3, 1997.

[48] G. Bowen, "Entanglement required in achieving entanglement-assisted channel capacities," *Physical Review A*, vol. 66, no. 5, 2002.

[49] T. Brun, I. Devetak, and M.-H. Hsieh, "Correcting quantum errors with entanglement," *Science*, vol. 314, no. 5798, pp. 436–439, 2006.

[50] M. M. Wilde and T. A. Brun, "Entanglement-assisted quantum convolutional coding," *Physical Review A*, vol. 81, no. 4, 2010.

[51] M. S. Postol, "A proposed quantum low density parity check code," *arXiv preprint quant-ph/0108131*, 2001.

[52] T. Camara, H. Ollivier, and J.-P. Tillich, "Constructions and performance of classes of quantum LDPC codes," *arXiv preprint quant-ph/0502086*, 2005.

[53] T. Camara, H. Ollivier, and J.-P. Tillich, "A class of quantum LDPC codes: Construction and performances under iterative decoding," in *Proceedings of IEEE International Symposium on Information Theory (ISIT), 2007*, pp. 811–815, 2007.

[54] M.-H. Hsieh, T. A. Brun, and I. Devetak, "Entanglement-assisted quantum quasicyclic low-density parity-check codes," *Physical Review A*, vol. 79, no. 3, 2009.

[55] Z. Babar, P. Botsinis, D. Alanis, S. X. Ng, and L. Hanzo, "Fifteen years of quantum LDPC coding and improved decoding strategies," *IEEE Access*, vol. 3, pp. 2492–2519, 2015.

[56] M. M. Wilde and M.-H. Hsieh, "Entanglement boosts quantum turbo codes," in *Proceedings of IEEE International Symposium on Information Theory (ISIT), 2011*, pp. 445–449, 2011.

[57] M. M. Wilde, M.-H. Hsieh, and Z. Babar, "Entanglement-assisted quantum turbo codes," *IEEE Transactions on Information Theory*, vol. 60, no. 2, pp. 1203–1222, 2014.

[58] Z. Babar, P. Botsinis, D. Alanis, S. X. Ng, and L. Hanzo, "The road from classical to quantum codes: A hashing bound approaching design procedure," *IEEE Access*, vol. 3, pp. 146–176, 2015.

[59] M. M. Wilde and J. M. Renes, "Quantum polar codes for arbitrary channels," in *Proceedings of IEEE International Symposium on Information Theory (ISIT), 2012*, pp. 334–338, 2012.

[60] J. Preskill, "Reliable quantum computers," *Proceedings of the Royal Society of London A: Mathematical, Physical and Engineering Sciences*, vol. 454, no. 1969, pp. 385–410, 1998.

[61] D. Gottesman, "Theory of fault-tolerant quantum computation," *Physical Review A*, vol. 57, no. 1, 1998.

[62] E. Knill, R. Laflamme, and W. H. Zurek, "Resilient quantum computation," *Science*, vol. 279, no. 5349, pp. 342–345, 1998.

[63] E. Knill, R. Laflamme, and W. H. Zurek, "Resilient quantum computation: error models and thresholds," *Proceedings of the Royal Society of London A: Mathematical, Physical and Engineering Sciences*, vol. 454, no. 1969, pp. 365–384, 1998.

[64] D. Gottesman, "Fault-tolerant quantum computation with constant overhead," *Quantum Information & Computation*, vol. 14, no. 15-16, pp. 1338–1372, 2014.

[65] J. Akhtman, R. Maunder, N. Bonello, and L. Hanzo, "Closed-form approximation of maximum free distance for binary block codes," in *Proceedings of IEEE 70th Vehicular Technology Conference Fall (VTC-Fall), 2009*, pp. 1–3, 2009.

[66] A. R. Calderbank and P. W. Shor, "Good quantum error-correcting codes exist," *Physical Review A*, vol. 54, no. 2, 1996.

[67] A. Steane, "Multiple-particle interference and quantum error correction," *Proceedings of the Royal Society of London A: Mathematical, Physical and Engineering Sciences*, vol. 452, no. 1954, pp. 2551–2577, 1996.

[68] P. A. M. Dirac, "A new notation for quantum mechanics," *Mathematical Proceedings of the Cambridge Philosophical Society*, vol. 35, no. 3, pp. 416–418, 1939.

[69] A. Ashikhmin, "Remarks on bounds for quantum codes," *arXiv preprint quant-ph/9705037*, 1997.

[70] P. Sarvepalli and A. Klappenecker, "Degenerate quantum codes and the quantum Hamming bound," *Physical Review A*, vol. 81, no. 3, 2010.

[71] M. A. Nielsen and I. L. Chuang, *Quantum computation and quantum information*. Cambridge University Press, 2000.

[72] P. Botsinis, Z. Babar, D. Alanis, D. Chandra, H. Nguyen, S. X. Ng, and L. Hanzo, "Quantum error correction protects quantum search algorithms against decoherence," *Scientific Reports*, vol. 6, 2016.

[73] R. Cleve and D. Gottesman, "Efficient computations of encodings for quantum error correction," *Physical Review A*, vol. 56, no. 1, 1997.

[74] I. Djordjevic, *Quantum information processing and quantum error correction: An engineering approach*. Academic Press, 2012.

[75] R. C. Singleton, "Maximum distance Q-nary codes," *IEEE Transactions on Information Theory*, vol. 10, no. 2, pp. 116–118, 1964.

[76] R. W. Hamming, "Error detecting and error correcting codes," *Bell System Technical Journal*, vol. 29, no. 2, pp. 147–160, 1950.

[77] E. N. Gilbert, "A comparison of signalling alphabets," *Bell System Technical Journal*, vol. 31, no. 3, pp. 504–522, 1952.

[78] E. Knill and R. Laflamme, "Theory of quantum error-correcting codes," *Physical Review A*, vol. 55, no. 2, 1997.

[79] R. J. McEliece, E. R. Rodemich, H. Rumsey Jr, and L. R. Welch, "New upper bounds on the rate of a code via the Delsarte-MacWilliams inequalities," *IEEE Transactions on Information Theory*, vol. 23, no. 2, pp. 157–166, 1977.

[80] M. Plotkin, "Binary codes with specified minimum distance," *IRE Transactions on Information Theory*, vol. 6, no. 4, pp. 445–450, 1960.

[81] E. M. Rains, "Quantum shadow enumerators," *IEEE Transactions on Information Theory*, vol. 45, no. 7, pp. 2361–2366, 1999.

[82] A. Ashikhmin and S. Litsyu, "Upper bounds on the size of quantum codes," *IEEE Transactions on Information Theory*, vol. 45, no. 4, pp. 1206–1215, 1999.

[83] C.-Y. Lai and C.-C. Lu, "A construction of quantum stabilizer codes based on syndrome assignment by classical parity-check matrices," *IEEE Transactions on Information Theory*, vol. 57, no. 10, pp. 7163–7179, 2011.

[84] Y. Xie, J. Yuan, *et al.*, "Design of quantum stabilizer codes from quadratic residues sets," *arXiv preprint arXiv:1407.8249*, 2014.

[85] M. Grassl, "Bounds on the minimum distance of linear codes and quantum codes." Online available at http://www.codetables.de, 2007. Accessed on 2017-05-01.

[86] C.-Y. Lai, "Linear programming bounds for entanglement-assisted quantum error-correcting codes by split weight enumerators," *arXiv preprint arXiv:1602.00413*, 2016.

[87] L. Guo and R. Li, "Linear Plotkin bound for entanglement-assisted quantum codes," *Physical Review A*, vol. 87, no. 3, 2013.

[88] C.-Y. Lai, T. A. Brun, and M. M. Wilde, "Dualities and identities for entanglement-assisted quantum codes," *Quantum Information Processing*, vol. 13, no. 4, pp. 957–990, 2014.

Daryus Chandra (S'15) received the M.Eng. degree in electrical engineering from Universitas Gadjah Mada, Indonesia, in 2014. He is currently pursuing the Ph.D. degree with the Southampton Wireless Group, School of Electronics and Computer Science, University of Southampton, UK. He is a recipient of scholarship award from the Indonesia Endowment Fund for Education (Lembaga Pengelola Dana Pendidikan, LPDP).

His research interests include classical and quantum error correction codes, quantum information, and quantum communications.

Zunaira Babar received her B.Eng. degree in electrical engineering from the National University of Science & Technology (NUST), Islamabad, Pakistan, in 2008, and the M.Sc. degree (Distinction) and the Ph.D degree in wireless communications from the University of Southampton, UK, in 2011 and 2015, respectively.

Her research interests include quantum error correction codes, channel coding, coded modulation, iterative detection and cooperative communications.

Hung Viet Nguyen received the B.Eng. degree in Electronics & Telecommunications from Hanoi University of Science and Technology (HUST), Hanoi, Vietnam, in 1999, the M.Eng. in Telecommunications from Asian Institute of Technology (AIT), Bangkok, Thailand, in 2002 and the Ph.D. degree in wireless communications from the University of Southampton, Southampton, U.K., in 2013. Since 1999 he has been a lecturer at the Post & Telecommunications Institute of Technology (PTIT), Vietnam. He is involved in the OPTIMIX and CONCERTO European projects. He is currently a postdoctoral researcher at Southampton Wireless (SW) group, University of Southampton, UK.

His research interests include cooperative communications, channel coding, network coding, and quantum communications.

Dimitrios Alanis (S'13) received the M.Eng. degree in Electrical and Computer Engineering from the Aristotle University of Thessaloniki in 2011 and the M.Sc. and PhD degrees in Wireless Communications from the University of Southampton in 2012 and 2017, respectively. He is currently working as a Research Fellow in Southampton Wireless (SW) group, School of Electronics and Computer Science of the University of Southampton, UK.

His research interests include quantum computation and quantum information theory, quantum search algorithms, cooperative communications, resource allocation for self-organizing networks, bio-inspired optimization algorithms and classical and quantum game theory.

Panagiotis Botsinis (S'12-M'16) received the M.Eng. degree from the School of Electrical and Computer Engineering of the National Technical University of Athens (NTUA), Greece, in 2010, as well as the M.Sc. degree with distinction and the Ph.D. degree in Wireless Communications from the University of Southampton, UK, in 2011 and 2015, respectively. He is currently working as a Research Fellow in the Southampton Wireless group at the School of Electronics and Computer Science of the University of Southampton, UK. Since October 2010, he has been a member of the Technical Chamber of Greece.

His research interests include quantum-assisted communications, quantum computation, iterative detection, OFDM, MIMO, multiple access systems, coded modulation, channel coding, cooperative communications, as well as combinatorial optimization.

Soon Xin Ng (S'99-M'03-SM'08) received the B.Eng. degree (First class) in electronic engineering and the Ph.D. degree in telecommunications from the University of Southampton, Southampton, U.K., in 1999 and 2002, respectively. From 2003 to 2006, he was a postdoctoral research fellow working on collaborative European research projects known as SCOUT, NEWCOM and PHOENIX. Since August 2006, he has been a member of academic staff in the School of Electronics and Computer Science, University of Southampton. He is involved in the OPTIMIX and CONCERTO European projects as well as the IU-ATC and UC4G projects. He is currently an Associate Professor in telecommunications at the University of Southampton.

His research interests include adaptive coded modulation, coded modulation, channel coding, space-time coding, joint source and channel coding, iterative detection, OFDM, MIMO, cooperative communications, distributed coding, quantum error correction codes and joint wireless-and-optical-fibre communications. He has published over 200 papers and co-authored two John Wiley/IEEE Press books in this field. He is a Senior Member of the IEEE, a Chartered Engineer and a Fellow of the Higher Education Academy in the UK.

Lajos Hanzo (M'91-SM'92-F'04) received his degree in electronics in 1976 and his doctorate in 1983. In 2009 he was awarded the honorary doctorate "Doctor Honoris Causa" by the Technical University of Budapest. During his 38-year career in telecommunications he has held various research and academic posts in Hungary, Germany and the UK. Since 1986 he has been with the School of Electronics and Computer Science, University of Southampton, UK, where he holds the chair in telecommunications. He has successfully supervised about 100 PhD students, co-authored 20 John Wiley/IEEE Press books on mobile radio communications totalling in excess of 10 000 pages, published 1400+ research entries at IEEE Xplore, acted both as TPC and General Chair of IEEE conferences, presented keynote lectures and has been awarded a number of distinctions. Currently he is directing a 100-strong academic research team, working on a range of research projects in the field of wireless multimedia communications sponsored by industry, the Engineering and Physical Sciences Research Council (EPSRC) UK, the European Research Councils Advanced Fellow Grant and the Royal Societys Wolfson Research Merit Award. He is an enthusiastic supporter of industrial and academic liaison and he offers a range of industrial courses.

Lajos is a Fellow of the Royal Academy of Engineering, of the Institution of Engineering and Technology, and of the European Association for Signal Processing. He is also a Governor of the IEEE VTS. During 2008–2012 he was the Editor-in-Chief of the IEEE Press and a Chaired Professor also at Tsinghua University, Beijing. He has 30 000+ citations. For further information on research in progress and associated publications please refer to http://www.wireless.ecs.soton.ac.uk.